The 1986–2021 paroxysmal episodes at the summit craters of Mt. Etna: Insights into volcano dynamics and hazard

Daniele Andronico [a,*], Andrea Cannata [a,b], Giuseppe Di Grazia [a], Ferruccio Ferrari [a]

[a] *Istituto Nazionale di Geofisica e Vulcanologia, ~~Sezione di Catania~~ – Osservatorio Etneo, Piazza Roma 2, ~~95125~~ Catania, Italy*
[b] *Dipartimento di Scienze Biologiche, Geologiche e Ambientali-Sezione di Scienze della Terra, Università degli Studi di Catania, Catania, Italy*

ARTICLE INFO

ABSTRACT

Despite Mt. Etna's long-standing reputation as an effusive volcano, since 1986 there has been an evident increase in mid-intensity explosive eruptions from its summit craters, with more than 240 episodes, better known as paroxysms (otherwise called paroxysmal episodes). These are characterized by strong Strombolian to lava fountaining activity that lasts from tens of minutes to a few days, producing some km-high volcanic plumes and tephra fallouts up to hundreds of km on the ground. Most paroxysms give life to sequences which are clustered like "episodic" eruptions for periods of a few days to a few months, their frequent recurrence causing hazard to air traffic and impacting densely inhabited areas. Nonetheless, a list containing the dates and data of these eruptions is lacking.

In this paper, we tried to fill this gap by compiling a complete record, including master data (date, crater), eruption style and seismic parameters for identifying, characterizing and quantifying both the individual episodes and the entire period. This information comes from a critical review of surveillance reports, raw-data analysis and scientific literature. A retrieval of homogenous and comparable seismic data was possible only for episodes after 2006 following the renewal of seismic stations.

The eruption list provides a complete picture of the 1986–2021 paroxysms, allowing to evaluate their temporal distribution, make a statistical analysis of their time-interval, and undertake a comprehensive investigation of the features of volcanic tremor. The results show a high probability (72%) of having a paroxysmal episode in the 10 days following the previous one. Moreover, a scaling relationship associated with the number-size distribution of the amplitude increases of volcanic tremor accompanying the explosive activities has been constrained. During sequences of paroxysms, combining these outputs can help improve the hazard assessment in terms of frequency of the associated tephra fallouts, and predict the duration of the entire sequence.

1. Introduction

Mt. Etna, in Sicily, Italy, has the reputation of being one of the most enduringly active volcanoes in the world. Based on the database on the Smithsonian Institution's Global Volcanism Program website, Etna counts the highest number of eruptions documented since the Holocene among the 25 volcanoes with the most recorded eruptions (Global Volcanism Program, 2013). A number of eruptions occurred especially in historical times (Guidoboni et al., 2014), with several of them witnessed in Greek and Roman times (Branca and Del Carlo, 2004). Looking at the historical catalogues of these authors and the recent geological map (Branca et al., 2011a), the dominant "effusive" feature of most of Etna's eruptions is quite striking. Of note are a number of high-intensity

explosive eruptions that formed thick tephra deposits from ~100 ka to the Present Coltelli et al., 2000), which are well-enough preserved to be recognizable around the volcano slopes, the 122 BCE Plinian eruption being the last powerful one (Coltelli et al., 1998).

Since 1986, there has been a clear growth in the number of mid-intensity explosive eruptions at Etna, culminating in the new millennium with two flank eruptions characterized by prolonged ash emission for weeks (in 2001) and months (2002–2003) (Taddeucci et al., 2002; Andronico et al., 2008a). During this time, 241 paroxysms, hereafter also called "paroxysmal episodes", took place from the summit craters (e.g. Andronico et al., 2015 and references therein; Corsaro et al., 2017) (Fig. 1). Most of these episodes were clustered within sequences lasting weeks to months, which have been termed "episodic eruptions"
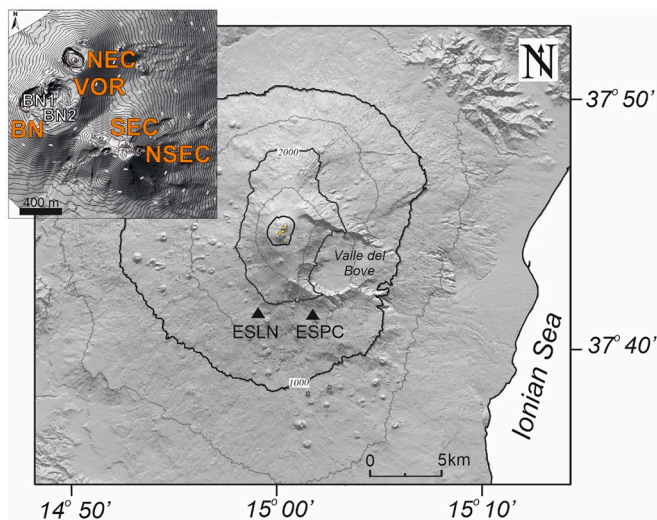
Fig. 1. Digital elevation model of Mt. Etna showing the locations of the two seismic stations used in this work. The inset in the left upper corner shows the digital elevation model of the summit area (VOR, Voragine; BN, Bocca Nuova (subdivided in two main crater sectors, BN1 and BN2); NEC, North-East Crater; SEC, South-East Crater; NSEC, New South-East Crater; from Neri et al., 2017).

(Andronico and Corsaro, 2011). At the time of writing, the last sequence was just recently, lasting from 16 February 2021 to 1 April 2021 and consisting of 17 episodes of lava fountains.

From a volcanic point of view, what makes paroxysms peculiar is the strong Strombolian and/or lava fountaining activity that lasts from a few hours to a few days overall, resulting in eruption columns rising up to 14 km a.s.l. (Corsaro et al., 2017). Thereafter, volcanic plumes extend until tens and, in some cases, hundreds of km away from the volcano (e.g. Andronico et al., 2014a, 2014b, 2015; Corsaro et al., 2017; Poret et al., 2018a, 2018b), causing moderate to light tephra fallouts at increasing distances between the proximal slopes and the most distal areas. Based on the eruption intensity, different degrees of damage can occur in both urban and rural areas. Major tephra fallouts can affect ground-based infrastructures, causing interruptions to the road traffic, damage to the rooves and gutters of houses, disruption to the normal course of everyday life, and even huge economic losses because of the damage to crops (Barnard, 2004). The most hazardous impact, however, is due to the injection of tephra into the atmosphere with potentially severe risks to aviation (e.g. Poret et al., 2018a, 2018b). Possible air-traffic disruption, ranging from the closure of air spaces over Etna up to the total closure of the regional airports (mainly the International Fontanarossa airport close to the town of Catania, ~27 km from the summit), can occur. Also, only recently another volcanic phenomenon, consisting of fallout of ballistic blocks and bombs, is considered a potential cause of high hazard during paroxysms within areas <5 km from the vent that can be visited daily by up to thousands of tourists (Andronico et al., 2015; Osman et al., 2019). Finally, the resuspension of ash in the inhabited areas, the cause of potential injuries also to human health, should not be overlooked (Andronico and Del Carlo, 2016; Horwell et al., 2017).

Despite their remarkable visibility and impact in the territory, a single catalogue containing dates and data of all these paroxysmal episodes is still lacking. In this paper, we tried to fill this gap by compiling a complete eruption list, where each paroxysmal episode occurring after 1986 is identified by master data (date and crater), volcanological observations on the eruption style and seismic features. On this latter, the need to use signals recorded by stations with similar sensors, together with the fact that the first permanent broadband seismic station was installed at Etna at the end of 2003, prevented performing seismic analyses on paroxysmal episodes that took place before that time. All of

this information has been drawn from research papers and the elaboration of raw data coming from the different institutions that have monitored Etna in the studied period (and possibly integrated by unpublished data). They are: Istituto Internazionale di Vulcanologia - Consiglio Nazionale delle Ricerche (1986–1999), Sistema Poseidon - Osservatorio Geodinamico Siciliano (1999–2001), and Istituto Nazionale di Geofisica e Vulcanologia, Osservatorio Etneo-Sezione di Catania (INGV-OE) since 2001. INGV-OE is the institution now in charge of seismic and volcanic monitoring in eastern Sicily, including the minor volcanic islands such as the Aeolian Islands and Pantelleria.

In the following, we first provide a complete framework of the recent explosive activity at Etna, focusing on the summit eruptions archived in our record and subdivided into six eruption types, of which only three were pertinent to our analysis. A description follows of the approach used for dealing with the whole dataset in terms of statistical analysis of the 1986–2021 paroxysmal episodes. We then present the INGV-OE seismic stations used in this work and define the seismic parameters and their cross-relationships used to characterize the time-series of episodes in 2006–2021.

By analysing the most recent 35-year-long explosive history of Etna, the different episodic eruptions have been characterized by evaluating the paroxysmal behaviour of Etna in terms of frequency, time-interval and temporal distribution of all the paroxysms. Lastly, we propose a scaling relationship associated with the number-size distribution of the amplitude increases of volcanic tremor accompanying the paroxysmal episodes in 2006–2021.

2. Volcanic activity at Etna

Since the Greek and Roman eras, the volcanic activity at Etna has been widely documented both in the summit and on its flanks (Branca and Del Carlo, 2004). In general, the summit of Etna consists of different sectors where effusive and explosive eruptions have taken place almost persistently. These eruptions can range considerably in terms of eruptive style, magnitude and intensity (Rittmann, 1973; Guest, 1982), continuously changing the morphology and stratigraphy of a summit area repeatedly affected by new tephra and lava deposits. The slopes of Etna, conversely, are mainly covered by extended lava flow fields, testifying to the almost purely effusive style that has dominated the volcanic activity of the last 2000 years (Branca et al., 2011a, 2011b). Some of these lava flows descended from the summit, but most are related to eruptive fissures breaking the flanks of the volcano at altitudes between 475 m and 2990 m, where also more than 300 cones have formed (Mazzarini and Armienti, 2001; Andronico and Lodato, 2005; Branca et al., 2011a). The moderately low recurrence of flank activity makes these lavas and cones visible and preserved for hundreds of years.

Today, Etna is a > 3300 m-high volcano with four summit craters, North-East Crater, Voragine, Bocca Nuova and South-East Crater, hereafter NEC, VOR, BN (currently composed of two main crater depressions, BN1 and BN2, respectively located in the NW and SE portions of the BN), and SEC, respectively (Fig. 1). They rise above a low-sloping area ranging approximately between 3000 m and 3100 m of elevation. In addition, a pit-crater, a few-meters across, has frequently been active on the east flank of the SEC cone since 2006, becoming continually erupting after 2009 (Andronico et al., 2013) and constituting the location of paroxysmal activity since 2011 (Behncke et al., 2014; De Beni et al., 2015), which caused the gradual growth of the New South-East Crater (NSEC; Fig. 1). Due to frequent eruptive activity, with time SEC and NSEC had increasingly merged as one (Andronico et al., 2018) enough to the disappearance of the clear morphological difference between the two cones, morphologically outlining a single apparatus. This is the reason for which INGV-OE very recently (i.e. in November 2020) decided to call the whole apparatus as the South-East Crater (SEC; INGV-OE, 2020a). In this work, however, we have continued to attribute the volcanic activity since that date to the NSEC for reasons of continuity with the younger cone. In addition, a thick rocky "septum" which

separated the VOR from the BN (Giammanco et al., 2007) partially collapsed on 12 January 2006 and then was almost totally destroyed by recent eruptions in 2015 and 2016 (Corsaro et al., 2017; Edwards et al., 2018). Both craters now form a nested structure, continuously changing in morphology, due to multiple collapses, growing scoria cones and lava accumulation (Corsaro et al., 2017). Finally, during the explosive activity that occurred in 2016 at the VOR and the NEC, the latter cone partially collapsed, forming an elongated-shaped depression (Edwards et al., 2018). From what has been described so far, it is clear that this is the summit area of Etna at the time of this work, but that the eruptive activity continuously and unpredictably changes the morphology of the craters.

Several authors have tried to frame the recent historical activity at Etna or even only during recent decades into "eruptive cycles". A long-term trend of increasing explosive activity at the summit and flank eruptions makes the 1670–2003 period still an on-going eruptive cycle for Branca and Del Carlo (2005). By analysing the effusive activity during the 20th Century, Andronico and Lodato (2005) argued that the 1971–1999 period shows a significant increase in eruption frequency associated with a large discharged lava volume and a higher effusion rate than the previous 1900–1971 interval. Based on relationships between the recharging of the plumbing system of the volcano and instability of its southeastern flanks, Allard et al. (2006) invoked a new eruptive cycle following the end of the 1991–1993 eruption (Calvari et al., 1994). Finally, Métrich et al. (2004) proposed an intense eruptive cycle initiated in the early 1970s by examining the chemistry and volatile content of olivine-hosted melt inclusions of products of the 2001 eruption.

Indeed, it is rather difficult to compare and analyse volcanic activity that several volcanologists have described over different centuries with different criteria, methodologies, detail and expertise. In the following, we focus only on the paroxysmal episodes occurring at the summit craters.

2.1. Paroxysmal activity at the summit craters

Improvements to the monitoring system over the last 20 years, especially video-camera and seismic networks (e.g. Andò and Pecora, 2006; Patanè et al., 2013), have enabled to detect, study and characterize the explosive activity at the summit of Etna with a detail previously never reached. It has also been shown how the evolution in time of paroxysms is accompanied by temporal changes in the volcanic tremor in terms of amplitude, spectral, polarization and source location features (e.g. Alparone et al., 2003, 2007a, 2007b; Cannata et al., 2008; Viccaro et al., 2014; Sciotto et al., 2019).

Based on volcanological observations, supported also by scientific literature and internal reports, we initially defined six eruption types (Table 1). Type 1 is represented by "Strombolian activity" (SA) which occurs within one of the summit craters forming a discontinuous, ephemeral gas plume with very low quantities of ash. The reference eruption type is weak Strombolian activity that on 8-9 November 2006 produced such a light fallout that ash was scarcely noticed by the residents in the higher villages on Etna (Andronico et al., 2009a). Type 2 describes a Strombolian episode (SE) producing a poorly ash-laden plume, associated with evident ash fall in the summit area but very light over the volcanic slopes, as occurred on 22 May 2020 (INGV-OE, 2020b). Type 3 is associated with intermediate activity between moderate "Strombolian explosions" (Type 2) and sustained lava fountains (Type 4). To define a clear delimitation of the two different and transient eruption styles, a classification scheme based on the duration of events (brief explosions versus prolonged fountains) has been proposed by Houghton et al. (2016). Here, we have called "transitional activity" (TA) an eruption type characterized by strong Strombolian activity alternating with short periods of lava fountains, which cause the formation of an eruption plume associated with moderate ash fallout. This eruption type is depicted well by the 24 November 2006 paroxysm, whose

Table 1

Eruption types classified based on volcanological observations and supported by scientific literature and/or internal reports carried out over more than 30 years of monitoring activity. The description of the eruption plume highlights the related/relative effects and difference in terms of erupted tephra.

Eruption type	Short title	Description of the eruption plume	Representative case	Reference (s)
1 - SA	Strombolian Activity	Discontinuous, ephemeral gas plume with very low quantities of ash	8-9 November 2006	Andronico et al., 2009a
2 - SE	Strombolian Episode	Poorly ash-laden plume, associated with evident ash fall in the summit area but very light over the volcanic slopes	22 May 2020	INGV-OE, 2020b
3 - TA	Transitional Activity	Strong Strombolian activity alternating with short periods of lava fountains, causing the formation of an eruption plume associated with moderate ash fallout	24 November 2006	Andronico et al., 2014a
4 - LF	Lava Fountain	Eruption plume spreading considerable ash and lapilli fallout over tens of kilometres from the vent	12–13 January 2011	Andronico et al., 2014b
5 - LSLF	Large-Scale Lava Fountain	Very high, dense eruption columns, followed by abundant coarse-grained tephra fallout down to the lower slopes of Etna and ash dispersal over hundreds of kilometres	23 February 2013 23 November 2013 3–5 December 2015	Poret et al., 2018a Poret et al., 2018b Corsaro et al., 2017
6 - SPF	Summit Paroxysm evolving into lateral Fissures	Temporary, short-lived eruption plumes both above the cone and along the main fissure opened in its flank, generating light to moderate tephra fallout	30 May – 5 June 2019	INGV-OE, 2019a, 2019b

explosive activity never completely evolved into continuous lava fountains (Andronico et al., 2014a). Type 4 consists of the best-known and common paroxysmal episodes at Etna, generating sustained "lava fountains" (LF) and, differently from the TA, an eruption plume causing considerable ash and lapilli fallout over tens of kilometres from the vent. The episode of 12–13 January 2011 is considered one of the most representative cases of lava fountains recorded on Etna (Andronico et al., 2014b). Type 5 includes "large-scale lava fountain" (LSLF) episodes of around an order of magnitude higher in terms of erupted tephra, as defined by Andronico et al. (2015). They are characterized by the rising of very high, dense eruption columns above the volcano, followed by abundant coarse-grained tephra fallout up to the lower slopes of Etna, ash dispersal up to hundreds of kilometres, and even the formation of

rheomorphic lava flows. The episodes on 23 February 2013 and 23 November 2013 at the NSEC (Poret et al., 2018a, 2018b) or on 3–5 December 2015 at the VOR (Corsaro et al., 2017) are recent examples well described in the literature. Lastly, Type 6 comprises strong Strombolian activity, accompanied or followed by the very rapid opening of vents/fissures along the flanks or at the base of the cone and this type of eruption is named "summit paroxysm evolving into lateral fissures" (SPF). It has been observed several times in recent years as, for example, during the eruption of May 2019 by the NSEC (INGV-OE, 2019a, 2019b), when light to moderate tephra fallout occurred during the first hours due to the formation of temporary, short-lived eruption plumes both above the cone and along the fissure. There was then a sharp decline until the end of the explosive activity, with lava output continuing on the fissure for a few days.

In this paper, we analysed all the increases of volcanic tremor amplitude time-related to the paroxysmal episodes that took place after 2006. We focused only on three eruption types, that involve lava fountaining as a threshold of explosive activity; lava fountains may contribute to the paroxysm alternating with strong Strombolian activity (type TA), or vary from sustained (type LF) to very sustained (type LSLF). In addition, all types share a trend of volcanic tremor that closely follows the evolution of the explosive phenomena, therefore their increase and decrease. In particular, the relationship between volcanic tremor amplitude and explosivity has allowed defining a common pattern for these types, schematically subdivided into three eruptive phases by Alparone et al. (2003). The *resumption phase* (1) marks the beginning of eruptive phenomena, usually consisting of episodic, low-intensity explosions that start to open the volcanic conduit. This phase, typically accompanied by a gradual increase in the volcanic tremor amplitude, can last from tens of minutes to a few days and can be followed by the emission of poor-fed lava flows. Gradually, the explosive activity grows from small bursts and ash puffs to weak Strombolian jets ejecting incandescent (coarse lapilli to bombs) molten clasts that fall back into or around the active vent(s). The Strombolian explosions increase in terms of frequency and intensity and thus the amount of ejected tephra, until evolving into the *paroxysmal phase* (2). During this phase, the eruptive style commonly consists of continuous to almost continuous lava fountains; these are gas jets propelling molten lava clots surrounded by a darker envelope of finer pyroclasts (Allard et al., 2005). However, a minor number of paroxysmal episodes (i.e. TA) alternate short periods of fountaining with prevalently highly frequent but discrete, strong Strombolian explosions. Whatever the dominant explosive style (strong Strombolian or lava fountaining), the fingerprint of the *paroxysmal phase* is the formation of an eruption column above the active vent made up of ash, lapilli and bomb-sized particles. These are first transported into atmosphere and then start to fall to the ground (from the coarser particles on the summit slopes to the finer ones in the distal areas). The volcanic tremor amplitude reaches its climax during the *paroxysmal phase*. The *conclusive phase* (3) signals the return to low levels of eruptive phenomena (both effusive and explosive) until their total exhaustion, while also the volcanic tremor amplitude returns to the background level preceding the beginning of the paroxysmal episode.

The two eruption styles that take part in the *paroxysmal phase*, namely lava fountaining and strong Strombolian activity, are clearly distinguishable by direct observation or camera recordings. This is well exemplified by the 4–5 September 2007 paroxysm, entirely characterized by lava fountains (Andronico et al., 2008b), and by the 24 November 2006 paroxysm, during which strong Strombolian activity alternated with short-length lava fountains (Polacci et al., 2009; Andronico et al., 2014b). Fig. 2 shows and compares the effects in the atmosphere of all the three eruption types in terms of eruption plume.

A similar eruptive behaviour of the summit paroxysmal activity has generally been observed at least since 1986, albeit with some exceptions and slight deviations from the general pattern. Hence, we managed to compile an eruption list of all the explosive activities recorded at the summit craters since 1986 (Table 2), that includes the eruption types TA, LF and LSLF. However, it is important to underline that the criteria adopted for our research necessarily forced us to exclude a number of explosive episodes. First, some "paroxysmal episodes" or "lava fountaining" at the BN in 1999, whose description in internal reports or scientific publications is overly brief or lacking in rigour from the volcanological point of view. As example, the explosive activity is defined as a lava fountain without any reference to the height and frequency of the magma jets or to the formation of an eruption column and the subsequent tephra fallout in the lower slopes of Etna. Therefore, the lack of clear "scientific" terms and descriptions consistent with our criteria does not allow inserting them in one of the three eruption types selected for this work (Harris and Neri, 2002; Behncke et al., 2003). Second, some "paroxysmal episodes" at the SEC in 2006 (Andronico et al., 2009b), for which volcanological observations suggest they belong to the SE type. This makes our final list conservative and therefore more reliable.

2.1.1. Discrete geophysical and geochemical measurements accompanying paroxysmal episodes

During paroxysmal episodes at Etna, several types of geophysical and geochemical measurements are performed and possibly integrated with each other, helping volcanologists to better understand the magma dynamics driving the related eruptive processes. According to measurements carried out using ground-based radars, during lava fountains the vertical velocities of magma jets can range between >80 m/s (average value of the entire eruptive jet; Dubosclard et al., 1999) and 250 m/s (for single ascending particles; Donnadieu et al., 2016). Estimations of SO_2 flux during lava fountains (or in between consecutive episodes which

Fig. 2. INGV-OE images from the CUAD surveillance camera located in Catania, showing examples of the three eruption types studied in this work: a) transitional activity - TA (19 April 2020); b) lava fountain – LF (18 March 2012); c) large-scale lava fountain – LSLF (23 November 2013).

Table 2

List of all the 1986–2021 paroxysmal episodes. We reported: cumulative number, date and time of maximum RD value, crater (VOR, Voragine; BN, Bocca Nuova; NEC, North-East Crater; SEC, South-East Crater; NSEC, New South-East Crater), eruption style (TA = Transitional Activity; LF = Lava Fountain; LSLF = Large-Scale Lava Fountain), RD_{MAX}, RD_{CUM}, shape factor f, tremor-derived duration and main reference(s) related to seismic date and data, eruption column height and related reference (s). When there are no seismic data providing an accurate time, the *next to the crater name indicates that the time of the Maximum RD value has been estimated by analysing the timing of the volcanological observations reported in the related reference. The only episode for which this estimation was not possible from literature, is the 4 September 1989 paroxysm. ˆ indicates that the height column is assumed to be "above the crater" by reading the description of the eruptive activity. The value of column height ">9" km evidences the upper limit of the INGV-OE camera system.

Cumulative number	Date | Maximum RD value	Crater	Eruption style	RD_{MAX} $\frac{cm^2 x}{cm}$	RD_{CUM} $\frac{cm^2 s}{scm^2 s}$	Shape Factor f	Duration hours	References	Column height km a.s.l.	References for the column height
1	24/09/1986 06:37	VOR*	LSLF					Gresta et al., 1996; Global Volcanism Program, 1986	9–10	Global Volcanism Program, 1986
2	04/05/1989 18:00	VOR*	LF					CNR-IIV, 1989a; Calvari et al., 1989		
3	29/08/1989 19:45	VOR*	LF					CNR-IIV, 1989b; Calvari et al., 1989		
4	04/09/1989 00:00	VOR*	LF					Branca and Del Carlo, 2004		
5	10/09/1989 10:50	VOR*	LF					CNR-IIV, 1989c; Calvari et al., 1989	>2ˆ	CNR-IIV, 1989d
6	11/09/1989 08:05	SEC	LF					Privitera et al., 2003		
7	11/09/1989 19:20	SEC	LF					Privitera et al., 2003		
8	12/09/1989 07:05	SEC	LF					Privitera et al., 2003		
9	12/09/1989 19:00	SEC	LF					Privitera et al., 2003		
10	13/09/1989 06:20	SEC	LF					Privitera et al., 2003	2ˆ	CNR-IIV, 1989d
11	13/09/1989 21:55	SEC	LF					Privitera et al., 2003		
12	19/09/1989 05:55	SEC	LF					Privitera et al., 2003	4–5ˆ	CNR-IIV, 1989d
13	22/09/1989 08:20	SEC	LF					Privitera et al., 2003	4ˆ	CNR-IIV, 1989d
14	22/09/1989 21:50	SEC	LF					Privitera et al., 2003		
15	23/09/1989 17:50	SEC	LF					Privitera et al., 2003	3ˆ	CNR-IIV, 1989d
16	24/09/1989 10:50	SEC	LF					Privitera et al., 2003	2ˆ	CNR-IIV, 1989d
17	25/09/1989 06:00	SEC	LF					Privitera et al., 2003	2ˆ	CNR-IIV, 1989d
18	25/09/1989 18:35	SEC	LF					Privitera et al., 2003		
19	26/09/1989 05:40	SEC	LF					Privitera et al., 2003	3ˆ	CNR-IIV, 1989d
20	26/09/1989 19:55	SEC	LF					Privitera et al., 2003		
21	27/09/1989 03:35	SEC	LF					Privitera et al., 2003		
22	05/01/1990 08:00	SEC*	LSLF					Carveni et al., 1994	15	Carveni et al., 1994
23	12/01/1990 10:30	SEC*	LF					Calvari et al., 1991		
24	15/01/1990 07:30	SEC*	LF					Calvari et al., 1991		
25	01/02/1990 21:30	SEC*	LF					Calvari et al., 1991		
26	07/08/1990 23:15	BN*	LF					Calvari et al., 1991		
27	09/11/1995 00:19	NEC*	LF					CNR-IIV, 1995		
28	10/11/1995 04:59	NEC*	LF					CNR-IIV, 1995	5	CNR-IIV, 1995
29	14/11/1995 08:35	NEC*	LF					CNR-IIV, 1995	5	CNR-IIV, 1995
30	23/11/1995 02:32	NEC*	LF					CNR-IIV, 1995		
31	27/11/1995 09:15	NEC*	LF					CNR-IIV, 1995		
32	23/12/1995 12:46	NEC*	LF					CNR-IIV, 1995	9.5 (6.2ˆ)	CNR-IIV, 1995
33		NEC*	LF					CNR-IIV, 1996a		

Table 2 (*continued*)

Cumulative number	Date | Maximum RD value	Crater	Eruption style	RD_{MAX} cm^2_X cm	RD_{CUM} $cm^2 s$ scm^2s	Shape Factor f	Duration *hours*	References	Column height *km a. s.l.*	References for the column height
	25/01/1996 08:00									
34	10/02/1996 00:52	NEC*	LF					CNR-IIV, 1996a		
35	06/06/1996 17:42	NEC*	LF					CNR-IIV, 1996b		
36	25/06/1996 23:00	NEC*	LF					CNR-IIV, 1996b		
37	28/03/1998 00:40	NEC*	LF					CNR-IIV, 1998a		
38	22/07/1998 17:01	VOR*	LSLF					CNR-IIV, 1998b	12	Andronico et al., 1999
39	06/08/1998 06:21	VOR*	LF					CNR-IIV, 1998b		
40	15/09/1998 00:31	SEC	LF					CNR-IIV, 1998b; Alparone and Privitera, 2001		
41	18/09/1998 06:19	SEC	LF					CNR-IIV, 1998b; Alparone and Privitera, 2001		
42	20/09/1998 10:42	SEC	LF					CNR-IIV, 1998b; Alparone and Privitera, 2001		
43	24/09/1998 15:26	SEC	LF					CNR-IIV, 1998b; Alparone and Privitera, 2001		
44	29/09/1998 20:36	SEC	LF					CNR-IIV, 1998b; Alparone and Privitera, 2001		
45	05/10/1998 10:53	SEC	LF					CNR-IIV, 1998c; Alparone and Privitera, 2001		
46	11/10/1998 16:37	SEC	LF					CNR-IIV, 1998c; Alparone and Privitera, 2001		
47	17/10/1998 22:37	SEC	LF					CNR-IIV, 1998c; Alparone and Privitera, 2001		
48	24/10/1998 12:46	SEC	LF					CNR-IIV, 1998c; Alparone and Privitera, 2001		
49	31/10/1998 19:21	SEC	LF					CNR-IIV, 1998c; Alparone and Privitera, 2001		
50	07/11/1998 02:59	SEC	LF					CNR-IIV, 1998c; Alparone and Privitera, 2001		
51	18/11/1998 04:23	SEC	LF					CNR-IIV, 1998c; Alparone and Privitera, 2001		
52	29/11/1998 06:43	SEC	LF					CNR-IIV, 1998c; Alparone and Privitera, 2001		
53	13/12/1998 21:03	SEC	LF					CNR-IIV, 1998c; Alparone and Privitera, 2001		
54	28/12/1998 23:33	SEC	LF					CNR-IIV, 1998c; Alparone and Privitera, 2001		
55	05/01/1999 08:39	SEC	LF					CNR-IIV, 1999; Alparone and Privitera, 2001		
56	10/01/1999 00:47	SEC	LF					CNR-IIV, 1999; Alparone and Privitera, 2001		
57	13/01/1999 04:49	SEC	LF					CNR-IIV, 1999; Alparone and Privitera, 2001		
58	16/01/1999 00:59	SEC	LF					CNR-IIV, 1999; Alparone and Privitera, 2001		
59	18/01/1999 06:20	SEC	LF					CNR-IIV, 1999; Alparone and Privitera, 2001		

Table 2 (*continued*)

Cumulative number	Date | Maximum RD value	Crater	Eruption style	RD_{MAX} cm^2_X cm	RD_{CUM} $cm^2 s$ scm^2s	Shape Factor f	Duration *hours*	References	Column height *km a. s.l.*	References for the column height
60	20/01/1999 11:03	SEC	LF					CNR-IIV, 1999; Alparone and Privitera, 2001		
61	23/01/1999 04:08	SEC	LF					CNR-IIV, 1999; Alparone and Privitera, 2001		
62	04/02/1999 13:39	SEC	LF					CNR-IIV, 1999; Alparone and Privitera, 2001		
63	04/09/1999 19:02	VOR	LSLF					Cannata et al., 2008; Global Volcanism Program, 1999		
64	04/09/1999 22:10	SEC	LF					Cannata et al., 2008; Global Volcanism Program, 1999		
65	20/09/1999 04:35	BN	TA					Cannata et al., 2008		
66	21/10/1999 03:25	BN	TA					Cannata et al., 2008		
67	22/10/1999 00:00	BN	LF					Behncke, 2004		
68	27/10/1999 16:27	BN	LF					Cannata et al., 2008		
69	04/11/1999 00:00	BN	TA					Cannata et al., 2008		
70	26/01/2000 03:50	SEC	LF					Alparone et al., 2003		
71	29/01/2000 06:55	SEC	LF					Alparone et al., 2003		
72	01/02/2000 07:55	SEC	LF					Alparone et al., 2003		
73	02/02/2000 06:45	SEC	LF					Alparone et al., 2003		
74	03/02/2000 06:50	SEC	LF					Alparone et al., 2003		
75	04/02/2000 08:45	SEC	LF					Alparone et al., 2003		
76	04/02/2000 22:40	SEC	LF					Alparone et al., 2003		
77	05/02/2000 10:40	SEC	LF					Alparone et al., 2003		
78	06/02/2000 03:20	SEC	LF					Alparone et al., 2003		
79	06/02/2000 21:50	SEC	LF					Alparone et al., 2003		
80	07/02/2000 15:40	SEC	LF					Alparone et al., 2003	6.4	Alparone et al., 2003
81	08/02/2000 10:15	SEC	LF					Alparone et al., 2003		
82	08/02/2000 18:55	SEC	LF					Alparone et al., 2003		
83	09/02/2000 06:50	SEC	LF					Alparone et al., 2003		
84	09/02/2000 23:20	SEC	LF					Alparone et al., 2003		
85	10/02/2000 12:10	SEC	LF					Alparone et al., 2003		
86	11/02/2000 04:25	SEC	LF					Alparone et al., 2003		
87	11/02/2000 20:45	SEC	LF					Alparone et al., 2003		
88	12/02/2000 02:50	SEC	LF					Alparone et al., 2003		
89	12/02/2000 08:25	SEC	LF					Alparone et al., 2003		
90	12/02/2000 23:25	SEC	LF					Alparone et al., 2003		
91	13/02/2000 11:35	SEC	LF					Alparone et al., 2003		
92	14/02/2000 02:10	SEC	LF					Alparone et al., 2003	7.4	Alparone et al., 2003
93	14/02/2000 15:00	SEC	LF					Alparone et al., 2003		
94		SEC	LF					Alparone et al., 2003		

Table 2 (*continued*)

Cumulative number	Date | Maximum RD value	Crater	Eruption style	RD_{MAX} cm^2_X cm	RD_{CUM} cm^2 s scm^2s	Shape Factor f	Duration hours	References	Column height km a. s.l.	References for the column height
	15/02/2000 16:50									
95	16/02/2000 05:40	SEC	LF					Alparone et al., 2003		
96	16/02/2000 15:05	SEC	LF					Alparone et al., 2003	>6.2	Alparone et al., 2003
97	17/02/2000 04:00	SEC	LF					Alparone et al., 2003		
98	17/02/2000 12:05	SEC	LF					Alparone et al., 2003		
99	17/02/2000 20:30	SEC	LF					Alparone et al., 2003		
100	18/02/2000 06:40	SEC	LF					Alparone et al., 2003		
101	18/02/2000 15:35	SEC	LF					Alparone et al., 2003		
102	19/02/2000 07:55	SEC	LF					Alparone et al., 2003		
103	20/02/2000 03:00	SEC	LF					Alparone et al., 2003		
104	20/02/2000 15:45	SEC	LF					Alparone et al., 2003		
105	23/02/2000 02:30	SEC	LF					Alparone et al., 2003		
106	27/02/2000 06:40	SEC	LF					Alparone et al., 2003		
107	28/02/2000 14:55	SEC	LF					Alparone et al., 2003		
108	04/03/2000 01:45	SEC	LF					Alparone et al., 2003		
109	08/03/2000 06:35	SEC	LF					Alparone et al., 2003	6.2	Alparone et al., 2003
110	12/03/2000 11:35	SEC	LF					Alparone et al., 2003		
111	14/03/2000 05:50	SEC	LF					Alparone et al., 2003		
112	19/03/2000 00:10	SEC	LF					Alparone et al., 2003		
113	22/03/2000 18:15	SEC	LF					Alparone et al., 2003		
114	24/03/2000 18:30	SEC	LF					Alparone et al., 2003		
115	29/03/2000 19:00	SEC	LF					Alparone et al., 2003		
116	01/04/2000 07:40	SEC	LF					Alparone et al., 2003	6.2	Alparone et al., 2003
117	03/04/2000 12:30	SEC	LF					Alparone et al., 2003		
118	06/04/2000 09:50	SEC	LF					Alparone et al., 2003		
119	16/04/2000 09:20	SEC	LF					Alparone et al., 2003	9.2	Alparone et al., 2003
120	26/04/2000 04:15	SEC	LF					Alparone et al., 2003	8.2	Alparone et al., 2003
121	05/05/2000 11:50	SEC	LF					Alparone et al., 2003	8.2	Alparone et al., 2003
122	15/05/2000 09:00	SEC	LF					Alparone et al., 2003		
123	15/05/2000 20:35	SEC	LF					Alparone et al., 2003		
124	17/05/2000 21:05	SEC	LF					Alparone et al., 2003		
125	19/05/2000 21:25	SEC	LF					Alparone et al., 2003		
126	23/05/2000 01:40	SEC	LF					Alparone et al., 2003		
127	27/05/2000 18:30	SEC	LF					Alparone et al., 2003		
128	01/06/2000 00:45	SEC	LF					Alparone et al., 2003	8.7	Alparone et al., 2003
129	01/06/2000 18:25	SEC	LF					Alparone et al., 2003		
130	05/06/2000 03:35	SEC	LF					Alparone et al., 2003	7.2	Alparone et al., 2003

Table 2 (*continued*)

Cumulative number	Date | Maximum RD value	Crater	Eruption style	RD_{MAX} cm^2_X cm	RD_{CUM} $cm^2\ s$ scm^2s	Shape Factor f	Duration hours	References	Column height km a. s.l.	References for the column height
131	08/06/2000 10:35	SEC	LF					Alparone et al., 2003		
132	14/06/2000 05:50	SEC	LF					Alparone et al., 2003	7.7	Alparone et al., 2003
133	24/06/2000 15:00	SEC	LF					Alparone et al., 2003	7.2	Alparone et al., 2003
134	28/08/2000 06:50	SEC	LF					Alparone et al., 2007a		
135	29/08/2000 05:57	SEC	LF					Alparone et al., 2007a		
136	09/05/2001 17:30	SEC	TA					Alparone et al., 2007a		
137	06/06/2001 20:48	SEC	TA					Alparone et al., 2004		
138	08/06/2001 21:56	SEC	TA					Alparone et al., 2004		
139	10/06/2001 21:50	SEC	LF					Alparone et al., 2004		
140	12/06/2001 15:42	SEC	LF					La Spina et al., 2015		
141	15/06/2001 07:40	SEC	LF					La Spina et al., 2015		
142	17/06/2001 07:45	SEC	LF					La Spina et al., 2015		
143	19/06/2001 17:45	SEC	LF					La Spina et al., 2015		
144	22/06/2001 14:45	SEC	LF					La Spina et al., 2015		
145	24/06/2001 07:45	SEC	LF					La Spina et al., 2015		
146	27/06/2001 07:52	SEC	LF					La Spina et al., 2015		
147	30/06/2001 04:10	SEC	LF					Alparone et al., 2004		
148	04/07/2001 10:38	SEC	LF					La Spina et al., 2015		
149	07/07/2001 05:00	SEC	LF					La Spina et al., 2015		
150	12/07/2001 19:21	SEC	LF					La Spina et al., 2015		
151	16/07/2001 19:49	SEC	LF					Alparone et al., 2004		
152	16/11/2006 07:00	SEC	TA	109	1,752,044	0.74	10.7	This work	4.5	Andronico et al., 2009b
153	19/11/2006 05:40	SEC	TA	31	474,660	0.71	25.3	This work		
154	21/11/2006 15:30	SEC	TA	65	1,218,851	0.87	13.0	This work		
155	24/11/2006 04:40	SEC	TA	86	947,042	0.51	12.3	This work	5.4	Andronico et al., 2009a, 2014b
156	27/11/2006 10:50	SEC	TA	76	1,247,013	0.76	10.3	This work		
157	29/03/2007 06:00	SEC	LF	191	765,715	0.19	2.7	This work		
158	11/04/2007 01:30	SEC	LF	137	1,463,459	0.49	5.7	This work		
159	29/04/2007 21:00	SEC	LF	100	1,535,791	0.71	12.2	This work		
160	07/05/2007 02:20	SEC	TA	72	1,330,723	0.85	11.8	This work		
161	05/09/2007 02:50	SEC	LF	61	495,561	0.37	13.0	This work	5	Andronico et al., 2008b
162	23/11/2007 21:00	SEC	LF	139	1,208,567	0.40	7.2	This work		
163	10/05/2008 14:20	SEC	LF	137	1,266,774	0.43	4.8	This work		
164	12/01/2011 22:10	NSEC	LF	125	938,475	0.35	6.7	This work	9	Andronico et al., 2014a
165	18/02/2011 10:20	NSEC	LF	126	1,944,530	0.72	10.0	This work		
166	10/04/2011 12:10	NSEC	LF	176	1,991,269	0.52	12.5	This work	> 9.0	Scollo et al., 2014
167	12/05/2011 01:40	NSEC	LF	226	2,470,299	0.51	10.0	This work		

Table 2 (*continued*)

Cumulative number	Date | Maximum RD value	Crater	Eruption style	RD_{MAX} cm^2_X cm	RD_{CUM} $cm^2 s$ scm^2s	Shape Factor f	Duration *hours*	References	Column height *km a. s.l.*	References for the column height
168	09/07/2011 14:50	NSEC	LF	138	867,211	0.29	9.7	This work	> 9.0	Scollo et al., 2014
169	19/07/2011 01:10	NSEC	LF	133	1,099,615	0.38	5.7	This work		
170	25/07/2011 05:20	NSEC	LF	245	1,967,060	0.37	11.7	This work		
171	30/07/2011 20:20	NSEC	LF	157	1,304,503	0.38	4.0	This work		
172	05/08/2011 23:00	NSEC	LF	169	1,235,743	0.34	6.2	This work		
173	12/08/2011 09:50	NSEC	LF	181	1,090,169	0.28	6.8	This work	> 9.0	Scollo et al., 2014
174	20/08/2011 07:40	NSEC	LF	171	690,225	0.19	4.5	This work	> 9.0	Scollo et al., 2014
175	29/08/2011 04:40	NSEC	LF	139	609,180	0.20	6.2	This work	> 9.0	Scollo et al., 2014
176	08/09/2011 07:40	NSEC	LF	118	661,021	0.26	3.2	This work	> 9.0	Scollo et al., 2014
177	19/09/2011 12:50	NSEC	LF	159	857,917	0.25	6.7	This work	5.0 ± 0.5	Scollo et al., 2014
178	28/09/2011 19:50	NSEC	LF	196	613,015	0.15	6.0	This work		
179	08/10/2011 15:00	NSEC	LF	188	717,900	0.18	4.7	This work	7.5 ± 0.5	Scollo et al., 2014
180	23/10/2011 20:00	NSEC	LF	159	1,015,651	0.30	3.5	This work		
181	15/11/2011 11:50	NSEC	LF	130	699,669	0.25	4.2	This work	> 9.0	Scollo et al., 2014
182	05/01/2012 06:40	NSEC	LF	165	869,001	0.24	8.5	This work	> 9.0	Scollo et al., 2014
183	09/02/2012 04:10	NSEC	LF	116	1,626,631	0.65	12.7	This work	8.0 ± 0.5	Scollo et al., 2014
184	04/03/2012 08:00	NSEC	LF	148	983,968	0.31	5.8	This work		
185	18/03/2012 09:20	NSEC	LF	115	797,922	0.32	7.2	This work	> 9.0	Scollo et al., 2014
186	01/04/2012 03:30	NSEC	LF	180	856,680	0.22	6.5	This work		
187	12/04/2012 14:40	NSEC	LF	167	788,324	0.22	8.3	This work	8.0 ± 0.5	Scollo et al., 2014
188	24/04/2012 01:50	NSEC	LF	181	832,031	0.21	10.7	This work		
189	19/02/2013 04:30	NSEC	LF	212	648,384	0.14	5.5	This work		
190	20/02/2013 01:20	NSEC	LF	117	525,703	0.21	3.7	This work		
191	20/02/2013 13:30	NSEC	LF	96	617,822	0.30	3.3	This work		
192	21/02/2013 04:50	NSEC	LF	122	447,133	0.17	4.2	This work		
193	23/02/2013 19:20	NSEC	LSLF	158	751,198	0.22	5.2	This work	8.7–9.3	Poret et al., 2018b
194	28/02/2013 10:40	NSEC	LF	245	750,836	0.14	3.7	This work	> 9.0	Scollo et al., 2014
195	05/03/2013 23:50	NSEC	LF	153	702,555	0.21	4.7	This work		
196	16/03/2013 18:10	NSEC	LSLF	231	861,486	0.17	2.2	This work		
197	03/04/2013 14:40	NSEC	LF	387	2,530,553	0.30	6.5	This work	7.5 ± 0.5	Scollo et al., 2014
198	12/04/2013 07:20	NSEC	LF	176	3,281,172	0.86	25.0	This work	7.5 ± 0.5	Scollo et al., 2014
199	18/04/2013 13:10	NSEC	LF	205	1,915,455	0.43	12.7	This work	> 9.0	Scollo et al., 2014
200	20/04/2013 15:30	NSEC	LF	176	853,584	0.22	5.8	This work		
201	27/04/2013 17:00	NSEC	LF	382	4,217,359	0.51	5.3	This work	8.5 ± 0.5	Scollo et al., 2014
202	26/10/2013 07:40	NSEC	LF	217	3,240,224	0.69	12.7	This work	8	Corradini et al., 2018
203	11/11/2013 09:50	NSEC	LF	542	4,843,510	0.41	14.7	This work		
204	17/11/2013 02:10	NSEC	LF	441	6,290,659	0.66	11.0	This work		

Table 2 (*continued*)

Cumulative number	Date | Maximum RD value	Crater	Eruption style	RD_{MAX} cm^2_X cm	RD_{CUM} $cm^2 s$ $scm^2 s$	Shape Factor f	Duration *hours*	References	Column height *km a. s.l.*	References for the column height
205	23/11/2013 09:50	NSEC	LSLF	277	1,220,928	0.20	5.8	This work	8–9 11.3	Andronico et al., 2015 Poret et al., 2018a▲
206	28/11/2013 20:30	NSEC	LF	421	4,661,005	0.51	9.5	This work		
207	02/12/2013 22:20	NSEC	LF	378	2,608,265	0.32	8.5	This work		
208	15/12/2013 21:30	NSEC	TA	180	2,306,728	0.59	20.3	This work		
209	30/12/2013 01:30	NSEC	TA	126	1,799,156	0.66	35.3	This work		
210	16/06/2014 04:30	NSEC	TA	59	897,998	0.70	28.0	This work		
211	28/12/2014 18:20	NSEC	LF	298	2,046,647	0.32	5.3	This work		
212	03/12/2015 02:50	VOR	LSLF	84	460,893	0.25	9.0	This work	11.8 14–15	Corsaro et al., 2017 Vulpiani et al., 2016
213	04/12/2015 10:00	VOR	LSLF	149	996,201	0.31	2.7	This work	14.1 13.4	Corsaro et al., 2017 Vulpiani et al., 2016
214	04/12/2015 21:30	VOR	LSLF	132	1,086,581	0.38	2.3	This work	10.5 13.3	Corsaro et al., 2017 Vulpiani et al., 2016
215	05/12/2015 16:30	VOR	LSLF	131	1,493,952	0.53	4.7	This work	10.4 13	Corsaro et al., 2017 Vulpiani et al., 2016
216	18/05/2016 13:10	VOR	LF	157	1,454,466	0.43	3.3	This work	6.3–6.8	Edwards et al., 2018
217	19/05/2016 04:40	VOR	LF	154	1,752,635	0.53	6.8	This work	4.3	Edwards et al., 2018
218	21/05/2016 03:10	VOR	LF	145	1,326,371	0.42	6.2	This work	6.3	Edwards et al., 2018
219	27/02/2017 22:20	NSEC	TA	34	603,365	0.81	73.0	This work		
220	19/04/2020 07:20	NSEC	TA	41	369,693	0.41	9.8	This work	5	
221	13/12/2020 22:20	NSEC	TA	116	745,789	0.30	8.8	This work		
222	21/12/2020 09:30	NSEC	TA	115	559,773	0.23	2.2	This work		
223	22/12/2020 04:40	NSEC	TA	80	665,839	0.39	4.2	This work		
224	18/01/2021 20:40	NSEC	TA	54	433,923	0.37	3.2	This work		
225	16/02/2021 16:40	NSEC	LSLF	86	504,875	0.27	1.5	This work	10	VONA, 2021a
226	18/02/2021 00:20	NSEC	LF	155	653,099	0.20	3.3	This work		
227	19/02/2021 09:20	NSEC	LF	157	778,927	0.23	3.0	This work	10	VONA, 2021b
228	21/02/2021 00:50	NSEC	LF	212	1,585,727	0.35	6.7	This work		
229	23/02/2021 00:00	NSEC	LSLF	221	954,478	0.20	4.2	This work		
230	24/02/2021 21:10	NSEC	LF	200	1,307,355	0.30	6.2	This work		
231	28/02/2021 08:30	NSEC	LSLF	195	550,756	0.13	1.7	This work	>9	VONA, 2021c
232	02/03/2021 14:30	NSEC	LF	162	1,136,955	0.32	5.0	This work	9	VONA, 2021d
233	04/03/2021 09:20	NSEC	LSLF	191	1,085,336	0.26	3.8	This work	11	VONA, 2021e
234	07/03/2021 06:50	NSEC	LSLF	255	994,426	0.18	6.5	This work	5	VONA, 2021f
235	10/03/2021 02:10	NSEC	LF	236	1,862,567	0.37	5.5	This work	7.5	VONA, 2021g
236	12/03/2021 09:40	NSEC	LSLF	236	1,972,190	0.39	8.0	This work	9	VONA, 2021h
237	15/03/2021 00:40	NSEC	LF	320	2,157,390	0.31	5.5	This work		
238	17/03/2021 04:20	NSEC	LF	276	2,638,378	0.44	6.2	This work		
239	19/03/2021 09:30	NSEC	LSLF	323	2,302,995	0.33	6.2	This work		
240	24/03/2021 02:40	NSEC	LF	276	4,445,677	0.74	13.5	This work	6	VONA, 2021i
241	01/04/2021 06:40	NSEC	LF	189	2,368,642	0.58	14.8	This work	9	VONA, 2021j

occur within interval times of 1–2 days) proved highly variable, i.e. from hundreds t/d to >20,000 t/d (Bonaccorso et al., 2011; Spampinato et al., 2015; Salerno et al., 2018). By using open-path Fourier transform infrared (OP-FTIR) spectrometry at ~1–2 km distance from the SEC, measurements of the magmatic gas phase accompanying lava fountaining showed CO_2-rich gas release, with CO_2/SO_2 and CO_2/HCl ratios peaking in coincidence with maxima in seismic tremor and fountain height (La Spina et al., 2015). Finally, high precision strainmeters have also been used to detect the volume of fluid and tephra involved during paroxysmal episodes, constrain the depth of the deformation source and infer on the evolution of sequence of paroxysms based on the decreasing trend of erupted tephra with time (Bonaccorso and Calvari, 2017).

2.1.2. The classification of paroxysmal episodes

Explosive eruptions are classified using the VEI (volcanic explosivity index), which ranges from 0 (non-explosive) to 8 (very large) based on the combination of several volcanological parameters, the chief of which are erupted tephra volume and plume height (Newhall and Self, 1982). Actually, although widely used and strategically very useful to compare explosive eruptions from the same volcano or among different volcanoes, such a classification has several shortcomings, as well evidenced by Bonadonna et al. (2016). This is particularly true for small-moderate eruptions, such as at Etna, for which it is very difficult to estimate both the total volume of tephra (distal fallout plus proximal deposits around the vent above the cone) erupted during the same paroxysm (Andronico et al., 2018). Moreover, based on the Newhall and Self classification scheme, even the range of plume heights (up to 14 km above sea level) displayed by eruption types TA, LF and LSLF is not crucial to discriminate different VEI values. For this reason, there is great uncertainty in assigning a VEI to the studied paroxysms, which can fluctuate between 2 and 3, with considerable ambiguity in the correct definition of erupted volume to attribute a VEI of 4, and therefore we have avoided this.

2.2. Other eruption categories

During the investigated period, Etna produced a high number of eruptions excluded from our study since they do not fall into one of the previous six aforementioned categories (Table 1). Table 3 summarises the main 1986–2021 flank and subterminal eruptions based on high emitted lava/tephra volumes or peculiar eruptive dynamics (e.g. intense ground deformation and volcano-tectonic activity for the 2018 short-lived effusive eruption; Cannavo et al., 2019; Laiolo et al., 2019), where "subterminal" refers to eruptions that affect the low slopes of the summit cones.

With regard to the eruptive activity taking place along fissures which open on the flanks of Etna, the explosive activity is less frequent compared to the summit paroxysmal episodes, and characterized by different dynamics and evolution of the eruptive phenomena. First of all, unlike the paroxysms, flank eruptions are preceded by seismic swarms. These herald the magma ascent to the surface along a path diverging from the central conduit in the upper volcanic edifice (e.g. Di Grazia et al., 2009; Cannavo et al., 2019). Secondly, in the case of intense and prolonged Strombolian activity, the accumulation of tephra can build a scoria cone(s) around the fissure vent(s) (Bottari et al., 1975; Spina et al., 2017). Only episodically, does an eruption column form above the cone, the 2001 and 2002–03 flank eruptions being the most recent ones that caused prolonged distal tephra fallout almost continuously for weeks and months (Taddeucci et al., 2002; Scollo et al., 2007; Andronico et al., 2008a). For these reasons, flank eruptions are excluded from our study.

3. Methods

3.1. Data collection and statistical analysis

Table 2 shows the list of the 241 paroxysms occurring at the summit craters since 1986, including cumulative number, date of the episode, time of maximum reduced displacement (RD) value (see the "Seismic parameters" subchapter), crater, eruption style, RD_{MAX}, RD_{CUM}, shape factor f and tremor-derived duration (see Section 3.2 for details), source of seismic data, column height and relative source. On the seismic data, for the episodes before 2006, we reported the main reference(s) from which we retrieved the time of maximum RD or peak activity, while for the episodes after 2006 the time of maximum RD value has been recalculated in this work by using the INGV-OE databank. As stated before, the analysis of volcanic tremor was performed only on the paroxysmal episodes from the end of 2003, and then RD_{MAX}, RD_{CUM}, shape factor and duration were provided since that date. The eruption style of each episode has been carefully assigned based on, or correlating with each other, descriptions from the literature, INGV-OE internal reports or websites, direct observations and the experience gained over more than 20 years of volcanic monitoring and surveillance by the authors. Concerning the column height above sea level during the paroxysm, over time this value has been estimated by different methods (evaluation of distal pictures, direct observations and surveillance camera images, satellite data, modelling through field data inversion,

Table 3

Summary of the main flank/subterminal eruptions mainly producing lava deposits and secondarily tephra from 1986 to 2019 in between sequences of paroxysms. The references cited are the main publications dealing with the indicated eruptions to the best of our knowledge. In italics, the most important erupted tephra volumes are reported. *indicates that the reported value is derived from the paper itself; ˆ indicates that the volume value includes both tephra and lava products. NEC = North-East Crater; SEC = South-East Crater; NSEC = New South-East Crater; VdB = Valle del Bove.

Year	Date	Type of activity	Vent location	Volume estimation $10^6 \, m^3$	References
1986–1987	30 October 1986–1 March 1987	Flank/subterminal eruption	Eastern flank: VdB, SEC	60	Romano, 1989
1989	11 September – 9 October	Flank/subterminal eruption	Eastern flank: VdB, SEC	38.4	Ferrucci et al., 1993a
1991–1993	14 December 1991–31 March 1993	Flank eruption	Eastern flank: VdB	235	Calvari et al., 1994
2001	17 July −9 August	Flank eruption	S and E flanks	40.1	Coltelli et al., 2007
				>1.75* (distal tephra)	*Scollo et al., 2007
				7.50 (scoria cone)	De Beni et al., 2020
2002–2003	26 October 2002–28 January 2003	Flank/ eruption	SSE and NNE flanks	77–96*ˆ	Andronico et al., 2005
					* Andronico et al., 2008a
2004–2005	7 September 2004–8 March 2005	Flank eruption	Eastern flank: VdB	63.3 ± 1.4	Fornaciai et al., 2005
2006	15–24 July	Subterminal eruption	SEC	2	Harris et al., 2011
2008–2009	13 May 2008–5 July 2009	Flank eruption	W wall of the VdB	74	Behncke et al., 2016
2014	22 January - 7 April	Subterminal eruption	NSEC	7.8	De Beni et al., 2015
2014	5 July - 10 August	Subterminal eruption	base of the NEC	8.6 ± 0.8ˆ	Bisson et al., 2021
2017	15 March – 27 April	Subterminal eruption	SE slope of the SEC	10.1	Cappello et al., 2019b
2018	24–27 December	Flank eruption	SE upper slope of VdB	2.25	Laiolo et al., 2019
2019	30 May – 6 June	Subterminal eruption	SE slope of the NSEC	4.40	De Beni et al., 2020

etc.). In particular, since 2020, the column heights calculated by using calibrated images collected by the INGV-OE video-surveillance system (visibility permitting) are inserted within the Volcano Observatory Notices for Aviation (VONA). These are succinct, plain-English messages aimed at dispatchers, pilots, and air-traffic controllers to inform them of volcanic unrest and eruptive activity that could produce ash-cloud hazards, which are sent to the Volcanic Ash Advisory Center (VAAC) located in Toulouse (France), and posted on the INGV website (https://www.ct.ingv.it/index.php/monitoraggio-e-sorveglianza/prodotti-del-monitoraggio/comunicati-vona).

For the purposes of this work, we assume (from a volcanological view) that a sequence of paroxysms takes place from the same crater, with at least three episodes within a short time-period (two weeks) or more than three. Moreover, we observe that episodes are separated by time–intervals up to 37 days in the 98% of cases (Table 4). However, in this work, we seek new insights in defining a sequence of paroxysms by analysing how the episodes tend to "cluster". To do so, we evaluated the time-series of two main parameters: the "time-interval", calculated as the time separating two consecutive paroxysms, and the "duration" of the single episodes, obtained by processing the homogenous seismic data carried out only for the episodes after 2006 (see the following subchapter for details).

3.2. Seismic parameters

The seismic stations used in this work belong to the permanent seismic network run by INGV-OE. We made use of the seismic signals recorded by two stations, ESPC and ESLN, located ~7 km from the centre of the summit area. These stations are equipped with broadband (40 s cut-off period), 3-component Trillium Nanometrics™ seismometers, acquiring at a sampling rate of 100 Hz (Fig. 1). In order to characterize the seismic behaviour of the considered paroxysms, we focused on the volcanic tremor amplitude.

The interval analysed for each episode has a duration of 6 h, 3 before and 3 after the time with the highest seismic amplitude. To define the amplitude of volcanic tremor during the paroxysms, we calculated: root mean square (RMS) amplitude and reduced displacement (RD). The RMS amplitudes were obtained by applying Parseval's theorem on the spectra of the vertical component of the seismic signals converted from velocity to displacement, calculated over 10.24-s-long windows, by the following equation (e.g. Battaglia and Aki, 2003):

$$RMS = \frac{1}{N}\sqrt{\sum_{k=0}^{N-1}|S_k|^2} \tag{1}$$

where S_k is the spectrum, and N is the number of spectral values falling

Table 4
Sequences of paroxysms as defined based on volcanological considerations, taking place at the five summit craters of Etna in the period 1989–2021.

Crater	Year(s)	Onset	End	N° episodes
VOR	1989	29 August 1989	10 September 1989	3
	2015	3 December 2015	5 December 2015	4
	2016	18 May 2016	21 May 2016	3
NEC	1995–1996	9 November 1995	25 June 1996	10
BN	1999	20 September 1999	4 November 1999	5
SEC	1989	11 September 1989	27 November 1989	16
	1990	5 January 1990	1 February 1990	4
	1998–1999	15 September 1998	4 February 1999	23
	2000	26 January 2000	24 June 2000	64
	2001	6 June 2001	16 July 2001	15
	2006	16 November 2006	27 November 2006	5
	2007	29 March 2007	7 May 2007	4
NSEC	2011–2012	12 January 2011	24 April 2012	25
	2013(a)	19 February 2013	27 April 2013	13
	2013(b)	26 October 2013	30 December 2013	8
	2021	16 February 2021	1 April 2021	17

in the frequency band of interest. In particular, such equation was applied in the band 0.5–2.5 Hz, as most of the volcanic tremor energy at Etna is comprised in this band (e.g. Cannata et al., 2008). To create more stable RMS amplitude time series, describing the pattern of volcanic tremor amplitude during each paroxysmal episode, the RMS values falling in 10-min-long windows were averaged.

Since the RMS amplitude depends not only on the intensity of the volcanic tremor source, but also on the distance between source and station (and then on the considered station and on the active vent location), we also calculated the RD, defined as a measure of the amplitude of volcanic tremor corrected for geometrical spreading and instrument magnification (Aki and Koyanagi, 1981). This parameter has been used to compare volcanic tremor amplitude recorded by different seismic stations during different eruptions at the same volcano, as well as on different volcanoes (e.g. McNutt, 1994; McNutt and Nishimura, 2008). In particular, assuming that the volcanic tremor wavefield is mainly composed of body waves, the following equation was used (Aki and Koyanagi, 1981):

$$RD = RMS\, r \tag{2}$$

where r is the source-station distance. In order to calculate r, as supported by previous studies (e.g. Patanè et al., 2008; Di Grazia et al., 2009; Viccaro et al., 2014) and shown by the near real-time locations routinely computed for surveillance purposes, the volcanic tremor source during the paroxysmal episodes was inferred to be located on the eruptive vent (SEC, NSEC, VOR or BN) at very shallow depth (3 km a.s. l.). For each episode we calculated RD time series, with the same time step as the RMS time series (10 min), and a peak value, called RD_{MAX} and defined as the maximum RD value within the time series (Fig. 3a). Also, a cumulative RD value was estimated to account not only for the maximum volcanic tremor amplitude but also for a fixed time window of the episode. Such parameter, called RD_{CUM}, was obtained by summing up all the values of each RD time series (Fig. 3b). Further, an additional parameter, called the shape factor and indicated by f, describing the shape of the RD time series (narrower or wider; Fig. 3c), was calculated as follows:

$$f = \frac{RD_{CUM}}{RD_{MAX}\cdot 21600} \tag{3}$$

where 21,600 represents the number of seconds within the 6-h-long windows, used to calculate RD_{CUM}. The higher the f value (ranging between 0 and 1), the wider the shape of the RD time series. Examples of paroxysmal episodes characterized by very different f values are shown in Fig. 4.

In order to quantify the duration of the episodes as objectively as possible, the pattern of volcanic tremor amplitude was taken into account. The STA/LTA (short time average/long time average) technique, routinely used in seismology to automatically pick the seismic phases of the earthquakes (e.g. Trnkoczy, 2012; D'Agostino et al., 2013), was applied on the RMS amplitude time series. The durations of the short and long-time windows were fixed to 1 and 12 h, the STA/LTA thresholds to declare the onset and the end of the episodes were chosen equal to 1.5 and 0.5, respectively (Fig. 3d).

To obtain the temporal evolution of the amplitude of the volcanic tremor during all the analysed paroxysmal episodes, as well as to allow comparisons, 48-h-long time series of RD values were extracted per each episode and merged to create a unique graph (Fig. 5). Unlike Fig. 3a where the RD_{MAX} values of episodes close-in-time have overlapped each other, Fig. 5 allows visualizing more clearly such data of all the episodes thereby enabling to identify eventual temporal evolutions in the amplitude of volcanic tremor recorded during sequences of episodes.

With the aim of acquiring information on the source mechanism of volcanic tremor recorded during paroxysmal episodes, its scaling relationships have been explored. In particular, we followed the approaches of other authors (e.g. Benoit et al., 2003; Sandanbata et al.,
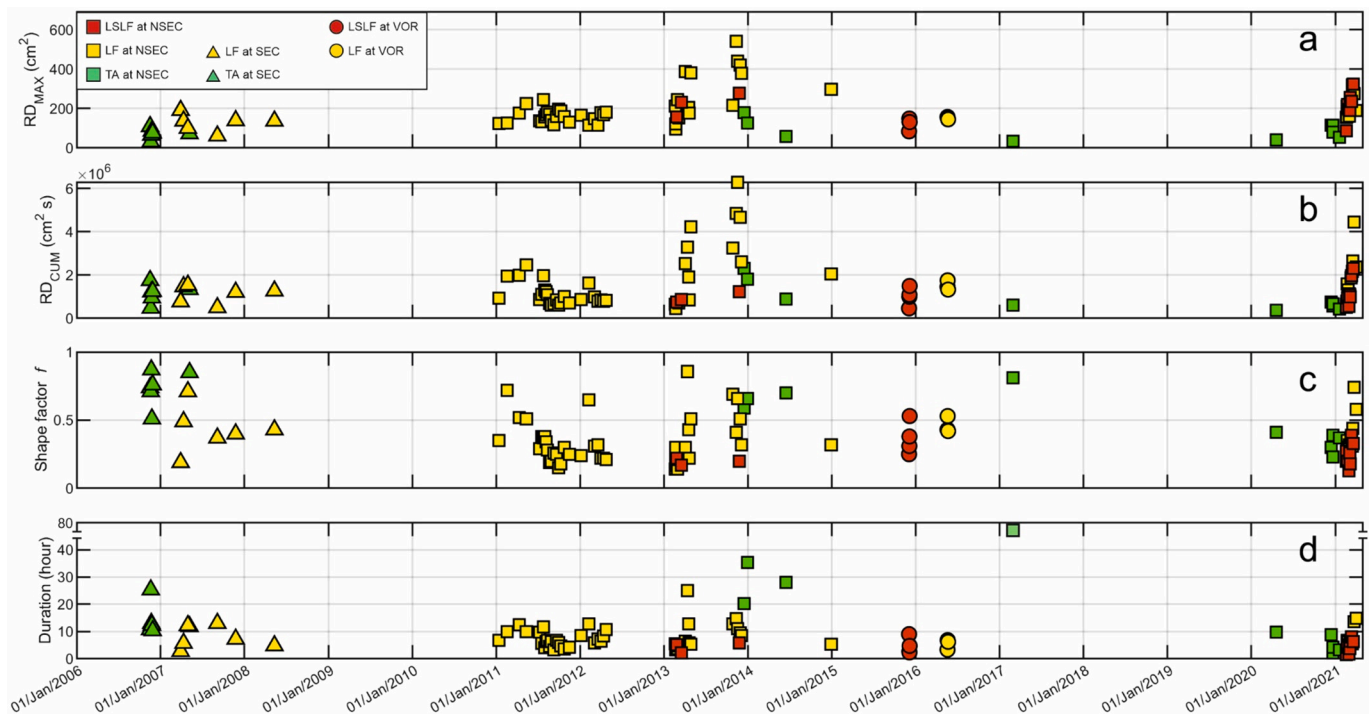
Fig. 3. Time series of (a) RD_{MAX}, (b) RD_{CUM}, (c) shape factor f, and (d) duration for different kinds of paroxysmal episodes taking place during 2006–2021 at distinct craters (see the key in the upper left corner of "a"). Note that the y-axis in (d) is cut to better represent the near totality of duration data.
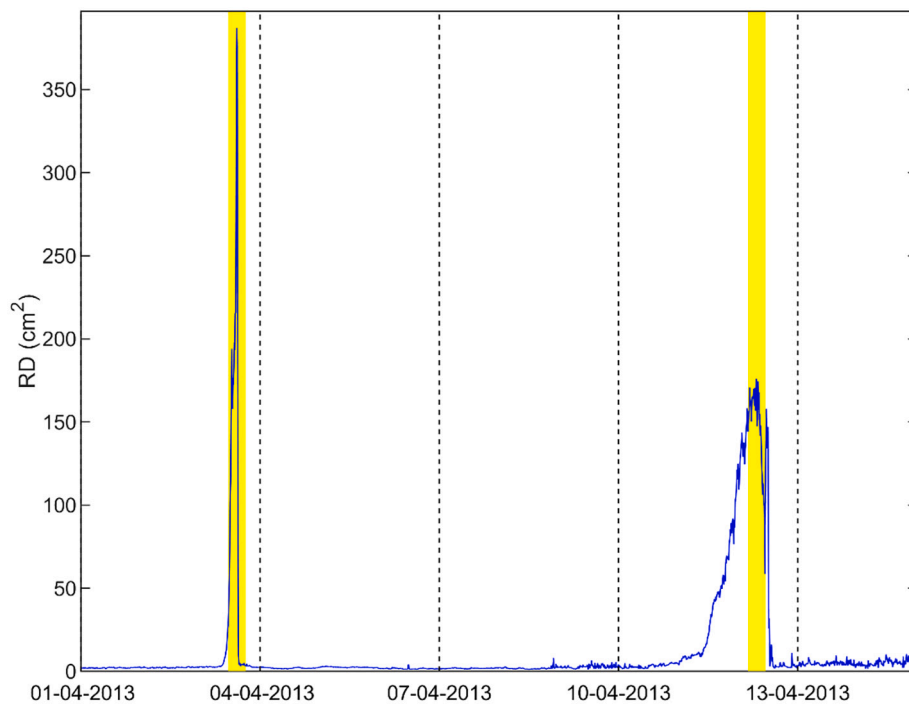

Fig. 4. Time series of RD obtained during 1–15 April 2013, when two consecutive paroxysmal episodes (both LF type at NSEC), characterized by different shape factors f (0.3 and 0.9 for 3 and 12 April episodes, respectively), took place. The yellow areas show the 6-h-long intervals used to estimate the shape factor f. (For interpretation of the references to colour in this figure legend, the reader is referred to the web version of this article.)

2015; Arámbula-Mendoza et al., 2016; Yukutake et al., 2017; Konstantinou et al., 2019), who investigated the duration-size distribution of volcanic tremor at different volcanoes. However, unlike the approach these authors took, due to the high number of paroxysms occurring at Etna, we considered their number in place of the duration. Hence, the scaling relationships associated with the number-size distribution was explored.

We tested two different distributions, exponential and power laws, considered as the most commonly used distributions to describe frequency-size relations in geophysics (e.g. Aki and Koyanagi, 1981; Benoit et al., 2003). The exponential law used to fit the data is as follows (e.g. Benoit et al., 2003):
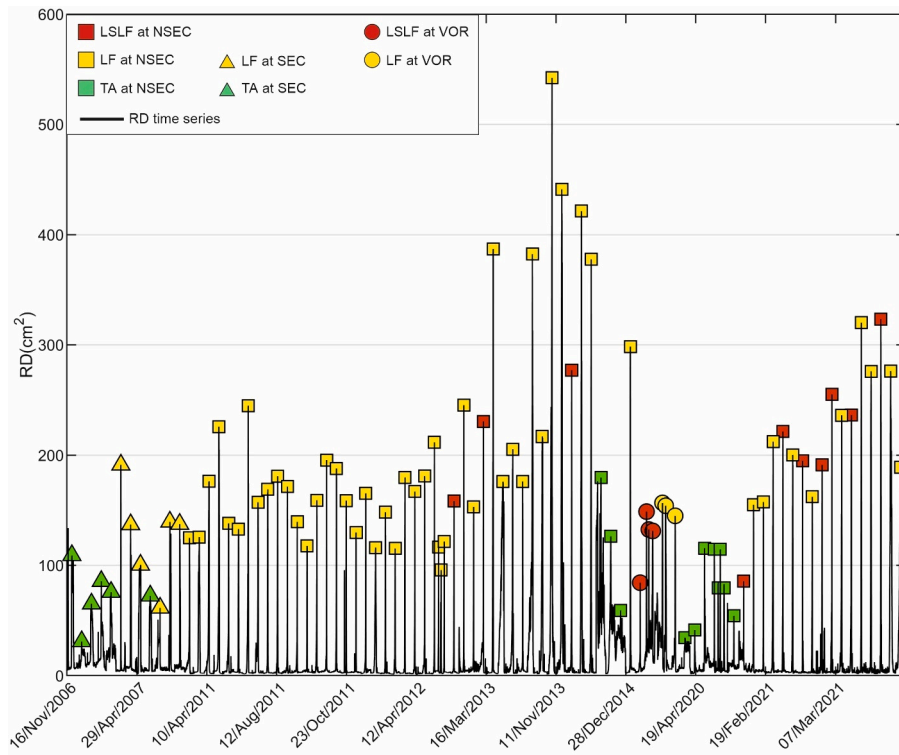
Fig. 5. 48-h-long time series of RD, extracted for each paroxysmal episode taking place during 2006–2021 and merged together to create a unique graph. The episodes were characterized by different explosivity and were generated by distinct craters (see the key in the upper left corner).

$$N_{RD_{MAX}} = N_t e^{-\lambda\, RD_{MAX}} \tag{4}$$

where $N_{RD_{MAX}}$ is the number of paroxysms with RD_{MAX} greater than or equal to a given value, N_t is the total number of paroxysms, and λ is the so-called scaling parameter. It should be noted that the inverse of λ (λ^{-1}) can be considered as the characteristic or mean amplitude of the distribution. This relationship can be linearized as (e.g. DeRoin et al., 2015):

$$log_{10}\left(\frac{N_{RD_{MAX}}}{N_t}\right) = -\lambda \frac{RD_{MAX}}{log_e(10)} \tag{5}$$

Thus, the exponential law is represented by a straight line in a lin-log graph (see black dashed line in Fig. 6a). On the other hand, the power law is (e.g. Benoit et al., 2003):

$$N_{RD_{MAX}} = N_t (RD_{MAX})^{-\gamma} \tag{6}$$

where γ is the slope of the power law line, corresponding to the "*b*-value" of the Gutenberg-Richter law (Gutenberg and Richter, 1954). This can
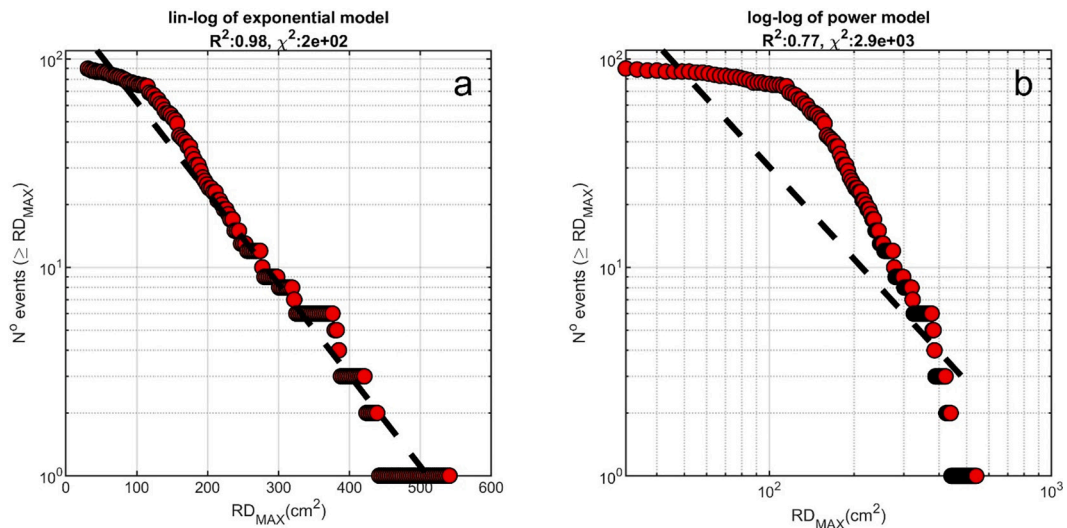
Fig. 6. Comparison between an exponential (a) and a power law (b) scaling model for the number of paroxysmal episodes versus RD_{MAX} distribution. The red dots show the observed data, while the dashed black lines the fits to exponential (a) and power law (b) models. Plots in (a) and (b) are lin-log and log-log, respectively. Information about the goodness of exponential and power law fits (R^2 and χ^2 statistic values) are reported in the plot titles. (For interpretation of the references to colour in this figure legend, the reader is referred to the web version of this article.)

be linearized as (e.g. DeRoin et al., 2015):

$$log_{10}\left(\frac{N_{RD_{MAX}}}{N_t}\right) = -\gamma log_{10}(RD_{MAX}) \tag{7}$$

The power law is represented by a straight line in a log-log graph (see black dashed line in Fig. 6b). Following Benoit et al. (2003), to evaluate the goodness of the fit of the distribution, two different methods were applied: computation of the coefficient of determination (R^2) and chi-square (χ^2) test. The former gives a measure of how well observed distributions are replicated by the model. The χ^2 test is used to understand how close the observed values are to those expected assuming a given distribution. The null hypothesis here is that the observed number-size distribution follows an exponential or power law. The χ^2 statistic is computed as follows:

$$\chi^2 = \sum_{i=1}^{n} \frac{(O_i - E_i)^2}{E_i} \tag{8}$$

where n is the number of classes in the number-size distribution, O_i is the observed frequency, and E_i is the expected frequency based on the exponential or power law models. If the χ^2 statistic is lower than a critical value, depending on the degrees of freedom and confidence level, there is no reason to reject the null hypothesis. Otherwise, if the χ^2 statistic is higher than the critical value, the considered models do not acceptably fit the observed number-size distribution.

4. Results

4.1. Statistical analysis

Fig. 7 shows the number of paroxysms per year from 1986 to 2021. Based on our definition of paroxysms, we counted 241 episodes, among which we classified 21 TA, 202 LF, and 18 LSLF. From a volcanological viewpoint, we have 16 sequences of paroxysms, which are listed in Table 4: seven at the SEC, four at the NSEC, three at the VOR, one each for BN and NEC. This equals 219 episodes (i.e. 91% of the total) in sequences that include from 3 to 64 episodes and cover periods lasting from 3 days to 16 months, while 22 episodes (9%) may be considered 'occasional'. Moreover, our analysis shows years during which paroxysms were highly frequent, i.e. in 1989, 1998–2001, 2011–2013 and 2021. Another well-known consideration is the high number of episodes from the SEC (57%) and the NSEC (30%) compared to the other craters, i.e 6% from the VOR and 5% and less than 3% from the NEC and the BN, respectively. Regarding eruption types, approximately 9% of the episodes are TA, 84% LF and 8% LSLF. However, looking solely at the 2006–2021 record, the TA episodes represent 17%, a value almost double compared to the 9% calculated for the 1986–2021 period. This suggests that the entire record may be underestimated because the TA paroxysms were not easily detectable before an enhancement of the permanent system of volcanic surveillance in terms of quantity and quality of cameras after 2004.

The chronological distribution of the time-interval between
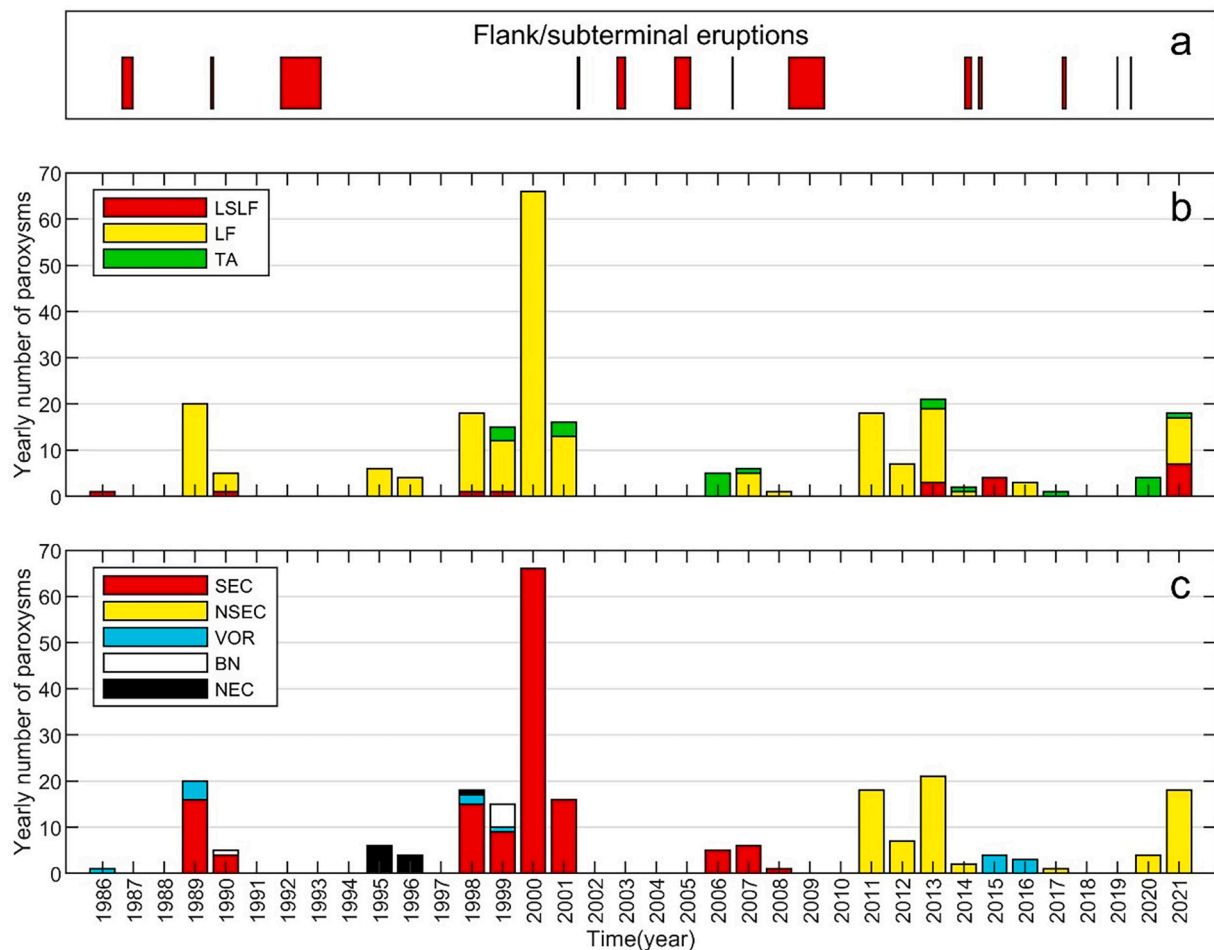
Fig. 7. Distribution of the paroxysmal episodes at the summit of Etna between 1986 and 2021. (a) The red bars mark the time when the main flank/eccentric eruptions occurred, usually in between sequences of paroxysms (see Table 4). (b) Stacked histogram showing the yearly number of paroxysmal episodes divided by type of activity. (c) Stacked histogram showing the yearly number of paroxysmal episodes divided by source crater. (For interpretation of the references to colour in this figure legend, the reader is referred to the web version of this article.)

consecutive episodes, calculated by the maximum tremor amplitude peaks, shows that no particular trend stands out when correlating the distribution of paroxysms with the overall period (Fig. 8). Conversely, similar patterns of gradual increase in the time-interval may have been observed within single sequences, e.g. in 2000 (Alparone et al., 2003), in the first sequence of 2013 (Spampinato et al., 2015) and in 2021.

All the episodes occurring in 1986–2021 are represented in Fig. 9 in two different ways. The red line shows the cumulative percentage of the total number of episodes vs. the duration of the time-interval between consecutive episodes; the cut-off is at the 49th class because the following classes are very scattered and include at most one episode. The blue bars display the frequency distribution of this duration; we observe that the longer the time-interval, the lower the percentage of paroxysms. The figure clearly shows most of the episodes occurred within 10 days following the previous episode (72%) and that the interval variability is extremely broad, i.e. from less than 12 h to more than 5 years including the time without paroxysmal episodes. In addition, the most populous frequency class of time-intervals is less than 1 day (55 episodes, corresponding to 23% of the total number). This pattern reflects a linear increase of the red line up to 6 days, followed by a progressive decrease in the slope and, after 17 days, by the almost levelling off the cumulative curve. In other words, Fig. 9 displays the rapid decreasing of the number of episodes from 23% (class = 1 day) down to 3% (class = 10 days), as consistently highlighted in the histogram of the percentage of time-interval.

Finally, Fig. 3d shows that most of the episodes show a tremor-derived duration ranging from 2 to 15 h. Looking at this parameter in detail (Fig. 10), we observe that TA episodes have higher duration variability, although most of them last 12 h, while LF typically last 6 h, with several episodes of 3, 9 and 12 h. The higher-intensity class of LSLF is not very representative due to the low number of episodes, however it generally shows a similar duration to LF, and never beyond 9 h. Moreover, TA overall have longer duration than most of LF and LSLF episodes, better represented by the average values showing even a clear
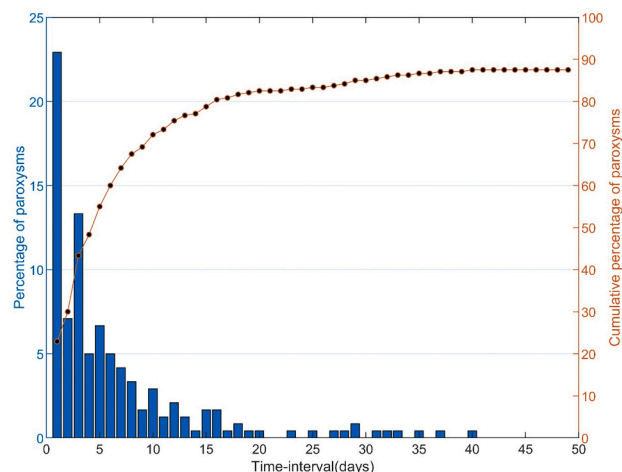
Fig. 9. Statistical analysis of all the paroxysmal episodes in the period 1986–2021 based on the time-interval between consecutive episodes. The bars correspond with the frequency values of such time-intervals (left y-axis), the red line and black dots show the cumulative percentage of the time-interval (right y-axis). The 100% value is reached at a value of time-interval of 1948 days. (For interpretation of the references to colour in this figure legend, the reader is referred to the web version of this article.)

decreasing pattern from TA (17.9 h) to LF (7.5 h) and LSLF (4.6 h).

4.2. Seismic analysis

For the 90 paroxysms since 2006, the values of RD_{MAX} range from 31 to 542 cm^2, while the values of RD_{CUM} from $3.70*10^5$ to $6.29*10^6$ cm^2 s (Fig. 3a, b). In particular, the maximum values of RD_{MAX} (~300–550 cm^2) were temporally clustered during 2013 (a few episodes also fall in 2021), while the minimum values (<100 cm^2) mainly during
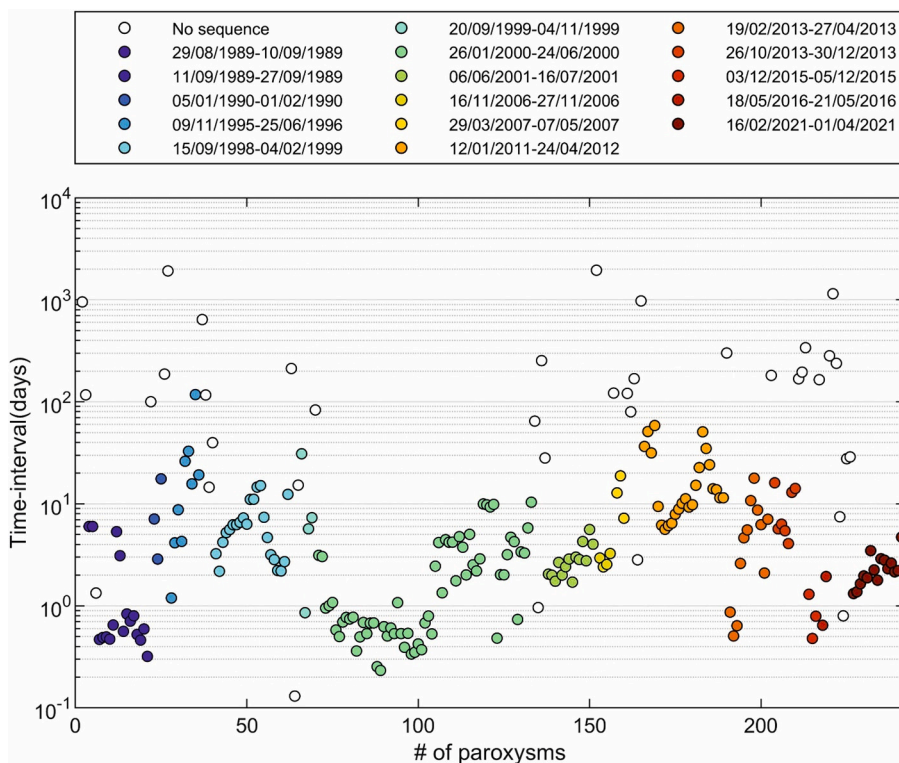

Fig. 8. Time-intervals between consecutive paroxysmal episodes versus the number of episodes between 1986 and 2021. Time-intervals within the same sequence have the same colour (see legend).
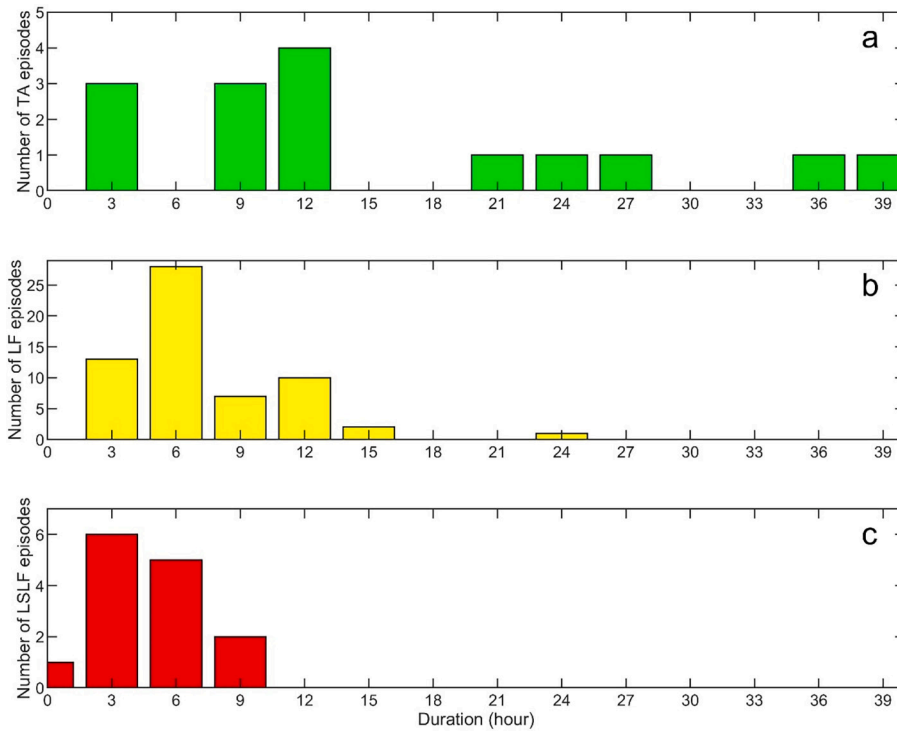
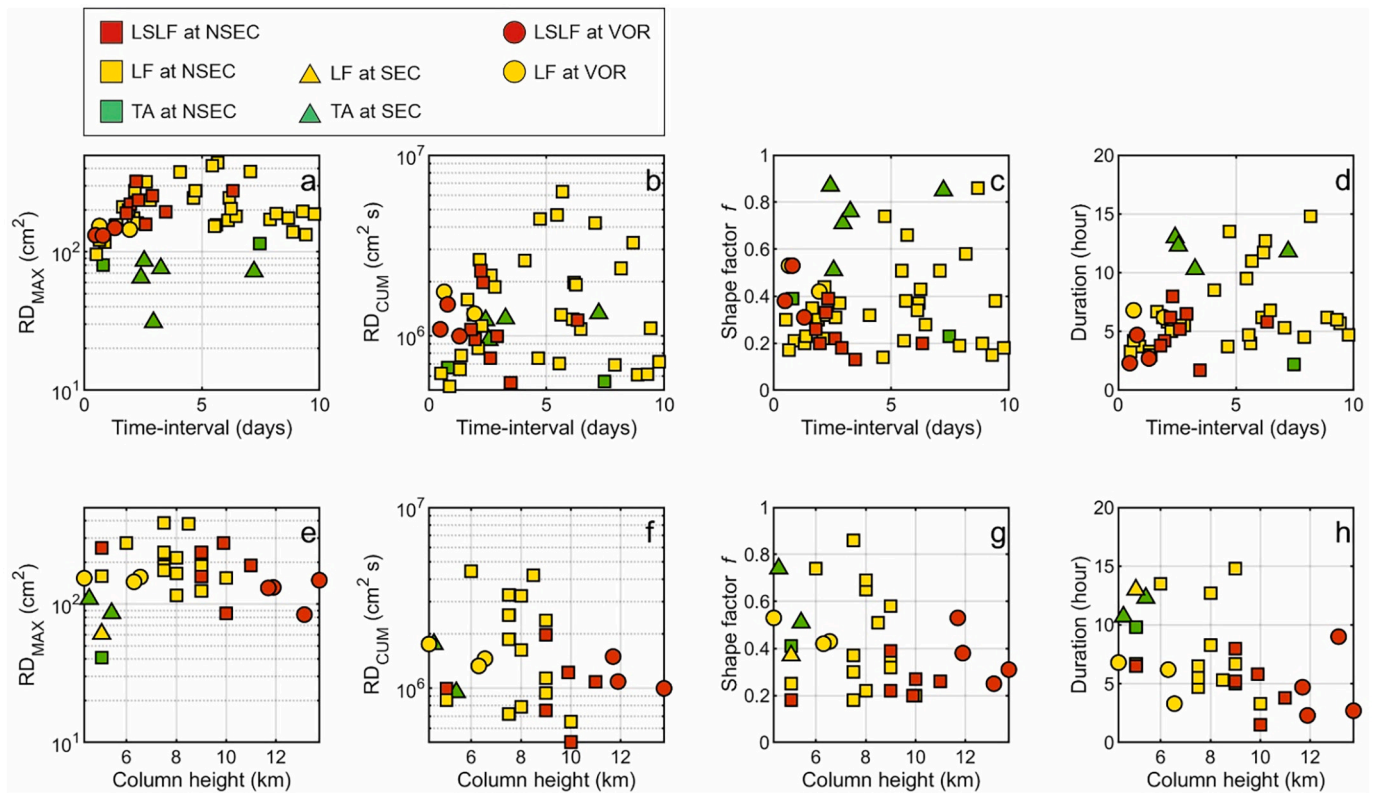**Fig. 10.** Frequency histogram of the duration (in hours) calculated for all the 2006–2021 paroxysmal episodes.

Fig. 11. (a) RD_{MAX}, (b) RD_{CUM}, (c) shape factor and (d) duration versus time-intervals between consecutive episodes, and (e) RD_{MAX}, (f) RD_{CUM}, (g) shape factor f and (h) duration versus column height (where such data are available) for different kinds of paroxysmal episodes taking place during 2006–2021 at distinct craters (see the key in the upper part of the plot). Regarding column height data (e-h), when more than one estimation was available the average value was calculated, while if the estimation was ">9" km, showing high uncertainty, such information was not used.

2006–2007 and after 2014. The highest RD_{MAX} and RD_{CUM} were observed during the episodes of 11 and 17 November 2013, respectively. Concerning the dependence of volcanic tremor amplitude from the source crater, we calculated mean and standard deviation values on RD_{MAX} and RD_{CUM} for each crater, that are equal to: 100 ± 44 cm^2 and $1.14*10^6 \pm 3.98*10^5$ cm^2 s for SEC, 193 ± 95 cm^2 and $1.50*10^6 \pm 1.19*10^6$ cm^2 s for NSEC and 136 ± 25 cm^2 and $1.22*10^6 \pm 4.22*10^5$ cm^2 s for VOR. As for the shape factor f, values ranging from 0.1 to 0.9 were obtained (Fig. 3c). It is worth noting that the episodes that took place during 2006 – onset of 2007 were characterized by high values of f, indicating a wide shape of the RD time series. On the other hand, the episodes from summer 2011 to the beginning of 2013 and during 2021 mainly showed low f values, suggesting a narrower shape of the RD time series. The remaining interval exhibited variable f values. However, despite the low number of TA episodes (compared to LF and LSLF) for a correct statistical analysis, it seems that the lower the intensity, the higher the f. As for the type of activities, it is worth noting that the minimum RD_{MAX} and RD_{CUM} were obtained during the TA. On the other hand, the maximum RD_{MAX} and RD_{CUM} values were not observed during the LSLF episodes.

Concerning the scaling relationships, Fig. 6 indicates that the exponential model is a better fit than the power law. This is also supported by the higher values of R^2 in the exponential model compared to the power law model (0.98 versus 0.77). In addition, the χ^2 statistic values obtained for the exponential model (195) and power law model (2906) are lower and greater than the critical value (200, in case of a confidence level of 95%), respectively. This allows rejecting the power law model with a confidence level of 95%. Focusing on the exponential model, the λ^{-1} parameter, considered as the "characteristic amplitude" is equal to $\sim$99 cm^2.

Furthermore, we explored the relationship between the time-intervals between consecutive episodes and the volcanic tremor amplitude, in terms of RD_{MAX}, RD_{CUM}, shape factor f and tremor-derived duration (Fig. 11 a–d). In particular, since most episodes exhibit a time-interval shorter than 10 days (72%; Fig. 9), we focused on the range 0–10 days. Finally, also the relationship between column height and the aforementioned volcanic tremor parameters was investigated (Fig. 11 e–h). Concerning the column height data, when more than one estimation was available the average value was calculated and plotted, while if the estimation was ">9" km, showing high uncertainty, such information was not used.

5. Discussion

5.1. Statistical analysis: a tool for understanding eruption dynamics?

The analysis of the long time-series of paroxysms (241 episodes) recorded in 35 years provides insights into the eruption dynamics which have governed the summit activity at Etna. First of all, most of the episodes (87%) took place at the SE summit sector of the volcano from the SEC and NSEC. Secondly, more than 90% of the total number of episodes highlights their predisposition to cluster together in sequences. In particular, we counted 16 sequences with at least three episodes; nine times out of 16 we recorded sequences made up of 8 or more episodes and, seven times, from 3 to 5 episodes.

In the past, Andronico and Corsaro (2011) defined the sequence of 64 lava fountains at the SEC in 2000 as an "episodic eruption", a term that also implies a systematic behaviour of the plumbing system which feeds the eruptive activity, triggering each single paroxysm one after the other. These authors suggested the periodic collapse of a foam layer accumulated at the top of the SEC reservoir and its rebuilding prior to each episode (Jaupart and Vergniolle, 1988, 1989; Vergniolle and Jaupart, 1990; Vergniolle, 1996). This mechanism was also invoked by Allard et al. (2005) and, for the 15 episodes-long sequence in 2001, by La Spina et al. (2015), in which the increased CO$_2$ supply to the shallow (2 km-deep) magma SEC reservoir is believed to be responsible for the

periodic growth and collapse of the bubble foam that feeds the episodic eruptions. Based on petro-compositional data of products erupted during the 2000 high recurrence of episodes, Andronico and Corsaro (2011) also showed that the time-series was characterized, at a certain point, by the rise of a new, more primitive magma entering into the SEC reservoir.

The 2000 episodic eruption was by far the most numerous sequence. However, data shown in Fig. 8 suggest the shallow magma chamber that feeds a sequence of paroxysms tends to drain out at almost equal intervals, which corresponds to a fairly regular magma-output rate. Therefore, we believe that the different magma dynamics occurring in the shallow plumbing system can produce two main eruptive scenarios. In the simplest case, the sequence of paroxysms can stop after a low number of episodes (3–5) due to the rapid emptying of the magma chamber. But most of the time, the episodic activity consists of a higher number of episodes since it takes longer to empty the amount of magma in the chamber. In this second scenario, the rate of magma output can vary in time for different reasons, and the sequence may be subdivided into sub-sequences. For example, as proved during the 2000 sequence, it is possible that a new, deeper input of magma could refill the shallow reservoir and continue to feed the paroxysmal activity with a different frequency (Andronico and Corsaro, 2011). Alternatively, the partial emptying of the magma chamber could increase the time needed to form the foam layer at its upper portion and thus the time-interval between episodes. This case seems to have occurred even during the last, 2021 sequence, where the time-intervals of the last 2 episodes ($\sim$5 days and >7 days) were the longest during the 17 episode-long sequence, with the first 15 having an average time-interval of only 2.2 days.

However, it should be remembered that in the literature an alternative model to the collapsing foam layer has also been suggested to explain the lava fountaining activity. Parfitt and Wilson (1995), in fact, described as "transitional" eruptions those activities which simultaneously exhibit aspects/features of both Strombolian Hawaiian styles, which are considered the end-members of a continuum of basaltic activity. To describe the eruptive dynamics governing these two different explosive styles, a "rise speed dependent" model has been proposed, which does not entail the formation of a bubble foam at the top of the magma reservoir, but rather a rapid volatile exsolution during magma ascent in the conduit (Parfitt, 2004 and reference therein). The transition from Strombolian to Hawaiian styles, therefore, would depend on the magma rise speed (estimated at 0.01–0.1 m/s) and gas content, with the Strombolian activity occurring at much lower speeds than Hawaiian activity (Parfitt and Wilson, 1995; Parfitt, 2004). As a result, we do not exclude that the rise speed model may be the mechanism describing and controlling transitional activities (TA) and some lava fountains of Etna as an alternative to the bubble foam model. This could occur both during occasional paroxysms and during the last episodes of a few sequences of paroxysms, and thus also explain the distribution of paroxysms within sequences with a high number of episodes.

5.2. Volcanic tremor during paroxysms

The obtained RD_{MAX} values ($\sim$31–542 cm^2; Fig. 3a and Fig. 5) fall in the range 4–2380 cm^2, as highlighted by McNutt and Nishimura (2008), and obtained by analysing 24 eruptions at 18 volcanoes. On the basis of the literature, the variability in the estimated RD_{MAX} values mainly depends on the following inter-related factors: i) fluid exit velocity (e.g. Ichihara, 2016), ii) volcanic explosivity index (VEI; e.g. McNutt, 2005), iii) cross-sectional area of the vent (e.g. McNutt and Nishimura, 2008). In particular, Sciotto et al. (2019) showed a close relationship between the volcanic tremor amplitude and the height of the lava fountain during six lava fountain episodes at Etna in 2011–2012. The height of the lava fountain is proportional to the square of the fluid exit velocity at the vent (Wilson et al., 1980). In addition, by investigating the lava fountain episodes at Etna during 2011–2015, Calvari et al. (2018) found a fairly wide range of explosivity. On the other hand, as for the vent cross-

sectional area, since most of the episodes took place at only two vents (12 at SEC and 71 at NSEC) and showed temporally scattered volcanic tremor amplitudes, we exclude that the calculated range of RD_{MAX} values could be due to the variation in the eruptive vent size.

It is possible to observe a relationship between the RD_{MAX} values and the features of the eruptions, in terms of explosivity (Fig. 5). In particular, the TA are generally characterized by lower values compared to LF and LSLF. Indeed, if we do not take the different source vents into account, the RD value of 110 cm^2 corresponds to ~70° percentile of the TA RD_{MAX} values, while it is ~5° and 14° percentile among the LF and LSLF RD_{MAX} values, respectively. However, the same reasoning, involving a sort of explosivity-volcanic tremor amplitude scaling, does not seem to apply to LF and LSLF. Six out of fourteen LSLF RD_{MAX} values are lower than the median value of the LF RD_{MAX} values (~169 cm^2). It is no trivial matter to understand the causes of the lack of a clear explosivity – volcanic tremor amplitude relationship in the cases of LF and LSLF. First of all, it is necessary to take into account the different craters producing LSLF. Indeed, four out of fourteen LSLF are generated by the VOR (29%), while most of LF by the NSEC and the SEC (58 out of 61; 95%). It has been shown how the conditions of the uppermost part of the plumbing system, in terms of vent radius, presence of changes in the conduit section and/or plug obstructing the vent, in addition to magma features (gas content, viscosity, and so on) and tephra grain sizes, affect the efficiency in radiating elastic energy (e.g. Eaton et al., 1987; McNutt and Nishimura, 2008; Fee et al., 2017; Spina et al., 2019; Sciotto et al., 2019; Gestrich et al., 2020). Hence, it is realistic to consider the different vents as being characterized by different conditions of the plumbing system and hence different seismic efficiency. On the other hand, even the ten LSLF generated by the NSEC are not characterized by the highest RD_{MAX} values among the episodes produced by the NSEC. In this case, the lack of a clear explosivity – volcanic tremor amplitude relationship at the same vent could be related to the temporal variability in the above-mentioned vent/plumbing system conditions, causing a temporally variable seismic efficiency. Focusing on the dependence of RD_{MAX} and RD_{CUM} values from the source crater, more energetic volcanic tremor is generally radiated during NSEC and VOR episodes, compared to the SEC ones. This is also evident in Fig. 5, showing that the first episodes taken into account and generated by the SEC (2006–2008), have on average lower RD_{MAX} values than the following ones generated by the NSEC and VOR. In addition, Fig. 5 also shows a generally increasing pattern in RD_{MAX} values taking place during 2011–2013 and during 2021.

Furthermore, by comparing the time-intervals between consecutive paroxysmal episodes with the volcanic tremor features in terms of RD_{MAX}, RD_{CUM}, shape factor f and tremor-derived duration, it is possible to note that the shorter the time-intervals, the lower the RD_{CUM}, the shape factor and the duration (Fig. 11a–d). Hence, paroxysmal episodes taking place close in time are generally impulsive and then characterized by rapid waxing and waning phases compared to the episodes more distant in time that show a slower pattern. The impulsive episodes are also likely to be characterized by higher column height, as suggested by Fig. 11g, h showing that the highest columns are generally associated with low values of both shape factor and duration. Focusing on the RD_{MAX} versus time-interval plot and in particular on the time-interval range 0–5 days (Fig. 11a), it is also possible to note a slight increasing pattern, that is, the longer the time-interval the higher the RD_{MAX}. However, such a pattern is not evident in the remaining part of the plot (time-interval range 5–10 days). It should also be emphasized that, during basaltic activity, the vertical buoyancy velocity within volcanic plumes can be lower than the horizontal wind component. At Etna, whose paroxysms have often relative low mass eruption rates, this effect produces "weak" plumes (as opposed to "strong plumes" which rise unmodified by strong winds; Sparks et al., 1997). Consequently, the "plume bending" by wind can effectively reduce the rise height of volcanic plumes (Bursik, 2001; Folch et al., 2016, and references therein).

As for the scaling relationships of the volcanic tremor recorded during the paroxysmal episodes, the exponential model shows a better fit compared to the power law model (Fig. 6). This agrees with observations of volcanic tremor collected at many volcanoes and geothermal areas (e.g. Benoit et al., 2003; Yukutake et al., 2017; Konstantinou et al., 2019). The exponential scaling relationship suggests that the source process of volcanic tremor during paroxysmal episodes at Etna is scale bound, not scale invariant (Benoit et al., 2003). Following the idea of Benoit et al. (2003) and Yukutake et al. (2017), we suggest that such a source mechanism is likely to be characterized by a fixed geometry with variable forces exciting the elastic radiation and then the volcanic tremor. The fixed geometry is related to the size and structure of the plumbing system feeding the eruptive vents. In this respect, it should be noted that most of the considered episodes were produced by the SEC and NSEC (83 out of 90 episodes). The variable forces could be represented by the flows of gas-rich magma along the plumbing system during the paroxysmal episodes. In particular, the variability can be related to the flow rate. Indeed, studies dealing with the relationships between seismo-acoustic features and eruption source parameters (Ichihara, 2016 and references therein), as well as laboratory investigations (e.g. Dinardo et al., 2013; Spina et al., 2019), show how an increasing flow rate causes increases in the seismic amplitudes. On the basis of this interpretation, the characteristic amplitude (λ^{-1}; see Eqs. (4) and (5)), equal to ~99 cm^2, should refer to the fixed characteristic length or scale, related to the size and structure of the plumbing system.

5.3. Hazard considerations

Both the complete 1986–2021 list of paroxysmal episodes and the 2006–2021 subset, quantitatively characterized from a volcanic tremor point of view, represent a powerful tool for a statistical assessment of volcanic hazards from tephra emission in the atmosphere.

The temporal distribution of paroxysmal episodes (Fig. 7) shows, during periods characterized by their total or nearly total absence, that the volcanic activity is dominated by flank/subterminal, mostly effusive eruptions. This occurred in 1991–92, with the largest eruption of Etna in the last 300 years from a magma volume standpoint (followed by two years of magma recharge; Calvari et al., 1994). Then in 2001, when a flank-eccentric eruption (Coltelli et al., 2007) came after a sequence of paroxysms, then followed by the 2002–03 eruption (Andronico et al., 2008a). It also occurred in 2004–05 and in 2008–09, when two long-lasting effusive eruptions produced compound lava flow fields (Burton et al., 2005) in Valle del Bove (Fig. 1). Again in 2014, with a subterminal eruption at the base of the NEC (Spina et al., 2017), and in 2017, with six episodes of lava output within 2 months (the first one producing paroxysmal activity) from the lower slopes of the NSEC (Cappello et al., 2019a). Finally, in 2018, the short-lived year-end eruption that broke through the upper slopes of Etna (Cannavo et al., 2019) and in 2019, with several SA, SE and SPF eruptive activities (INGV-OE, 2019a, 2019b, 2019c).

Looking at Fig. 9, we can see that, given a paroxysm, the cumulative probability of having another episode within 24, 48 and 72 h is 23%, 30% and 43%, respectively, for the whole dataset. This means that, there is a 43% probability that another paroxysm will occur within the first 3 days, while the time after which the probability of having another episode is low and more or less the same is after 17 days, i.e. when the curve tends to flatten significantly. Interestingly, we obtained similar patterns and percentages also by separating i) the paroxysms based on the craters, i.e. SEC and NSEC on one hand and the other craters on the other, and ii) for two sub-sets of episodes, i.e. by temporally subdividing the whole dataset into two parts. These results prove that this eruptive dynamics is valid irrespective of the crater or the temporal distribution of the episodes.

Continuing on this line, these percentages may be used to forecast the onset of a new sequence of paroxysms. Indeed, the probability of occurrence of a paroxysmal episode is higher right after the occurrence of a previous episode (up to a few days) and then sharply decreases over time.

With regard to the explosivity, it is possible to observe how the TA are generally characterized by lower values of RD_{MAX} compared to LF and LSLF. Therefore, the amplitude of volcanic tremor can be used as a tool to discriminate these types of activities. This is especially useful when the summit part of the volcano is not directly visible owing to cloudy weather.

6. Concluding remarks

In general, volcanic surveillance is based on the ability to understand how volcanoes work and how their dynamics evolve during eruptions; therefore, the alert of imminent eruptions as well as the monitoring of the evolution of ongoing eruptive phenomena comply with the continuous progress of scientific knowledge. In Italy, in particular, repeated agreements have been made in recent years between INGV-OE and the national civil protection to establish procedures that pursue these objectives on Italian volcanoes. In this frame, our work marks an essential step forward in the knowledge of activity at Etna by evaluating the paroxysmal activity (updated until the 30 March-1 April 2021 paroxysm) taking place at the summit craters of Etna after 1986. Based on distinguishing volcanological features, six different eruption types were first classified; we then compiled a list of 241 episodes related to the three most intense eruption types, which include transitional activity (alternating strong Strombolian and fountaining styles), lava fountains and large-scale lava fountains. Such a dataset, supported by seismic and time parameters, allowed obtaining a robust statistical and seismic examination of each episode and a better comprehension of the eruptive pattern during sequences of paroxysms lasting weeks to months.

Our analysis shows a clusterization of 91% of the paroxysmal episodes over 16 sequences, and the time-interval does not exceed 10 days for 72% of the episodes. This value is also an estimation of the probability of having another episode within 10 days after a paroxysm. Therefore, relationships between consecutive episodes may be an effective tool for assessing the hazard from paroxysms and providing their probability of occurrence. From a strictly seismic viewpoint, we obtained an exponential scale-law fitting the number-size distribution of amplitude increases of volcanic tremor accompanying the paroxysms, suggesting how the source process of tremor during such paroxysmal episodes is scale bound, not scale invariant. Furthermore, the amplitude of volcanic tremor proved an effective tool to discriminate transitional activity (on one hand) and lava fountains and large-scale lava fountains (on the other hand).

For the future, we plan to convert these records into an accessible database, upgradable in near real-time in case of new paroxysmal activity, capable of displaying different types of graphs and updating the statistical analysis of the paroxysmal activity at Etna. To reduce the uncertainty of our analysis, we are planning further work to recover seismic data from 1998 to 2001 and hence compare the 114 paroxysmal episodes, that occurred in this period, with the ones taking place in 2006–2021. It would allow expanding the dataset and improving both the seismic and statistical analyses. Finally, our results may help better comprehend the relationships between explosive eruptions and volcanic tremor on other volcanoes with similar eruptive activity to Etna.

Declaration of Competing Interest

Daniele Andronico, Andrea Cannata, Giuseppe Di Grazia and Ferruccio Ferrari declare no Conflict of Interest for the realization of the paper submitted to Earth-Science Reviews, entitled "The 1986–2020 paroxysmal episodes at the summit craters of Mt Etna: insights into volcano dynamics and hazard".

Acknowledgements

References

Aki, K., Koyanagi, R., 1981. Deep volcanic tremor and magma ascent mechanism under Kilauea, Hawaii. J. Geophys. Res. 86, 7095–7109. https://doi.org/10.1029/JB086iB08p07095.

Allard, P., Burton, M., Murè, F., 2005. Spectroscopic evidence for a lava fountain driven by previously accumulated magmatic gas. Nature 433, 407–410. https://doi.org/10.1038/nature03246.

Allard, P., Behncke, B., D'Amico, S., Neri, M., Gambino, S., 2006. Mount Etna 1993–2005: anatomy of an evolving eruptive cycle. Earth Sci. Rev. 78, 85–114. https://doi.org/10.1016/j.earscirev.2006.04.002.

Alparone, S., Privitera, E., 2001. Characteristics of the intermittent volcanic tremor at Mt. Etna, Italy, during the 15 September 1998–4 February 1999 eruptive episode. In: Proc. of Cities on Volcanoes 2 Conference, Auckland, New Zealand, 12th–16th February 2001, Earthquake Commission, Inst. Geol. Nucl. Sci. Inf. Ser, 49. Inst. of Geol. And Nucl. Sci. Lower Hutt, New Zealand.

Alparone, S., Andronico, D., Lodato, L., Sgroi, T., 2003. Relationship between tremor and volcanic activity during the Southeast Crater eruption on Mount Etna in early 2000. J. Geophys. Res. 108 (B5), 2241. https://doi.org/10.1029/2002JB001866.

Alparone, S., Andronico, D., Sgroi, T., 2004. Characteristics of the volcanic tremor at Southeast Crater, Etna (Italy), during a long series of explosive paroxysms. In: IAVCEI General Assembly 2004, Pucón – Chile, November 14–19.

Alparone, S., Andronico, D., Sgroi, T., Ferrari, F., Lodato, L., Reitano, D., 2007a. Alert system to mitigate tephra fallout hazards at Mt. Etna Volcano, Italy. Nat. Hazards 43, 333–350. https://doi.org/10.1007/s11069-007-9120-7.

Alparone, S., Cannata, A., Gresta, S., 2007b. Time variation of spectral and wavefield features of volcanic tremor at Mt. Etna (January–June 1999). J. Volcanol. Geotherm. Res. 161, 318–332. https://doi.org/10.1016/j.jvolgeores.2006.12.012.

Andò, B., Pecora, E., 2006. An advanced video-based system for monitoring active volcanoes. Comput. Geosci. 32, 85–91. https://doi.org/10.1016/j.cageo.2005.05.004.

Andronico, D., Del Carlo, P., Coltelli, M., (1999). The 22 July 1998 fire fountain episode at Voragine Crater (Mt. Etna, Italy). Proceedings of the Volcanic and Magmatic Studies Group—Annual Meeting. January 5–6, 1999.

Andronico, D., Corsaro, R.A., 2011. Lava fountains during the episodic eruption of South–East Crater (Mt. Etna), 2000: insights into magma-gas dynamics within the shallow volcano plumbing system. Bull. Volcanol. 73 (9), 1165–1178. https://doi.org/10.1007/s00445-011-0467-y.

Andronico, D., Del Carlo, P., 2016. PM_{10} measurements in urban settlements after lava fountain episodes at Mt. Etna, Italy: pilot test to assess volcanic ash hazard on human health. Nat. Hazards Earth Syst. Sci. 16, 29–40. https://doi.org/10.5194/nhess-16-29-2016.

Andronico, D., Lodato, L., 2005. Effusive activity at Mount Etna Volcano (Italy) during the 20th Century: a contribution to volcanic hazard assessment. Nat. Hazards 36, 407–443. https://doi.org/10.1007/s11069-005-1938-2.

Andronico, D., Branca, S., Calvari, S., Burton, M., Caltabiano, T., Corsaro, R.A., Del Carlo, P., Garfì, G., Lodato, G., Miraglia, L., Murè, F., Neri, M., Pecora, E., Pompilio, M., Salerno, G., Spampinato, L., 2005. A multi-disciplinary study of the 2002–03 Etna eruption: insights into a complex plumbing system. Bull. Volcanol. 67, 314–330. https://doi.org/10.1007/s00445-004-0372-8.

Andronico, D., Scollo, S., Caruso, S., Cristaldi, A., 2008a. The 2002–03 Etna explosive activity: tephra dispersal and features of the deposits. J. Geophys. Res. 113, B04209 https://doi.org/10.1029/2007JB005126.

Andronico, D., Cristaldi, A., Scollo, S., 2008b. The 4–5 September 2007 lava fountain at South-East Crater of Mt Etna, Italy. J. Volcanol. Geotherm. Res. 173, 325–328. https://doi.org/10.1016/j.jvolgeores.2008.02.004.

Andronico, D., Spinetti, C., Cristaldi, A., Buongiorno, M.F., 2009a. Observations of Mt. Etna volcanic ash plumes in 2006: an integrated approach from ground-based and polar satellite NOAA-AVHRR monitoring system. J. Volcanol. Geotherm. Res. 180 (2–4), 135–147. https://doi.org/10.1016/j.jvolgeores.2008.11.013.

Andronico, D., Scollo, S., Cristaldi, A., Ferrari, F., 2009b. Monitoring ash emission episodes at Mt. Etna: the 16 November 2006 case study. J. Volcanol. Geotherm. Res. 180 (2–4), 123–134. https://doi.org/10.1016/j.jvolgeores.2008.10.019.

Andronico, D., Lo Castro, M.D., Sciotto, M., Spina, L., 2013. The 2010 ash emissions at the summit craters of Mt Etna: relationship with seismo-acoustic signals. J. Geophys. Res. Solid Earth 118, 51–70. https://doi.org/10.1029/2012JB009895.

Andronico, D., Scollo, S., Cristaldi, A., Lo Castro, M.D., 2014a. Representivity of incompletely sampled fall deposits in estimating eruption source parameters: a test using the 12–13 January 2011 lava fountain deposit from Mt. Etna volcano, Italy. Bull. Volcanol. 76, 861. https://doi.org/10.1007/s00445-014-0861-3.

Andronico, D., Scollo, S., Lo Castro, M.D., Cristaldi, A., Lodato, L., Taddeucci, J., 2014b. Eruption dynamics and tephra dispersal from the 24 November 2006 paroxysm at South-East Crater, Mt Etna, Italy. J. Volcanol. Geotherm. Res. 274, 78–91. https://doi.org/10.1016/j.jvolgeores.2014.01.009.

Andronico, D., Scollo, S., Cristaldi, A., 2015. Unexpected hazards from tephra fallouts at Mt Etna: the 23 November 2013 lava fountain. J. Volcanol. Geotherm. Res. 304, 118–125. https://doi.org/10.1016/j.jvolgeores.2015.08.007.

Andronico, D., Behncke, B., De Beni, E., Cristaldi, A., Scollo, S., Lopez, M., Lo Castro, M. D., 2018. Magma budget from lava and tephra volumes erupted during the 25–26 October 2013 lava fountain at Mt Etna. Front. Earth Sci. 6, 116. https://doi.org/10.3389/feart.2018.00116.

Arámbula-Mendoza, R., Valdés-González, C., Varley, N., Reyes-Pimentel, T.A., Juárez-García, B., 2016. Tremor and its duration-amplitude distribution at Popocatépetl volcano, Mexico. Geophys. Res. Lett. 43, 8994–9001. https://doi.org/10.1002/2016GL070227.

Barnard, S.T., 2004. Results of a reconnaissance trip to Mt. Etna, Italy: the effects of the 2002 eruption of Etna on the province of Catania. Bull. N. Z. Soc. Earthq. Eng. 37 (2), 47–62. https://doi.org/10.5459/bnzsee.37.2.47-61.

Battaglia, J., Aki, K., 2003. Location of seismic events and eruptive fissures on the Piton de la Fournaise volcano using seismic amplitudes. J. Geophys. Res. 108 (B8), 2364. https://doi.org/10.1029/2002JB002193.

Behncke, B., 2004. Italy's Volcanoes: the Cradle of Volcanology. At https://www.italysvolcanoes.com.

Behncke, B., Neri, M., Carniel, R., 2003. An exceptional case of endogenous lava dome growth spawning pyroclastic avalanches: the 1999 Bocca Nuova eruption of Mt. Etna (Italy). J. Volcanol. Geotherm. Res. 124, 115–128. https://doi.org/10.1016/S0377-0273(03)00072-6.

Behncke, B., Branca, S., Corsaro, R.A., De Beni, E., Miraglia, L., Proietti, P., 2014. The 2011–2012 summit activity of Mount Etna: birth, growth and products of the new SE crater. J. Volcanol. Geotherm. Res. 270, 10–21. https://doi.org/10.1016/j.jvolgeores.2013.11.012.

Behncke, B., Fornaciai, A., Neri, M., Favalli, M., Ganci, G., Mazzarini, F., 2016. Lidar surveys reveal eruptive volumes and rates at Etna, 2007–2010. Geophys. Res. Lett. 43, 4270–4278. https://doi.org/10.1002/2016GL068495.

Benoit, J.P., McNutt, S.R., Barboza, V., 2003. Duration-amplitude distribution of volcanic tremor. J. Geophys. Res. 108 (B3), 2146. https://doi.org/10.1029/2001JB001520.

Bisson, M., Spinetti, C., Andronico, D., Palaseanu-Lovejoy, M., Buongiorno, M.F., Alexandrov, O., Cecere, T., 2021. Ten years of volcanic activity at Mt Etna: high resolution mapping and accurate quantification of the morphological changes by Pleiades and Lidar data. International Journal of Applied Earth Observations and Geoinformation 102, 102369. https://doi.org/10.1016/j.jag.2021.102369.

Bonaccorso, A., Calvari, S., 2017. A new approach to investigate an eruptive paroxysmal sequence using camera and strainmeter networks: lessons from the 3–5 December 2015 activity at Etna volcano. Earth Planet. Sci. Lett. 475, 231–241. https://doi.org/10.1016/j.epsl.2017.07.020.

Bonaccorso, A., Caltabiano, T., Currenti, G., Del Negro, C., Gambino, S., Ganci, G., Giammanco, S., Greco, F., Pistorio, A., Salerno, G., Spampinato, S., Boschi, E., 2011. Dynamics of a lava fountain revealed by geophysical, geochemical and thermal satellite measurements: the case of 10 April 2011 Mt. Etna eruption. Geophys. Res. Lett. 38, L24307 https://doi.org/10.1029/2011GL049637.

Bonadonna, C., Cioni, R., Costa, A., Druitt, T., Phillips, J., Pioli, L., Andronico, D., Harris, A., Scollo, S., Bachmann, O., Bagheri, G., Biass, S., Brogi, E., Cashman, K., Dominguez, L., Durig, T., Galland, O., Giordano, G., Gudmundsson, M., Hort, M., Hoskuldsson, A., Houghton, B., Komorowski, J.C., Kuppers, U., Lacanna, G., Le Pennec, J.L., Macedonio, G., Manga, M., Manzella, I., de Michieli Vitturi, M., Neri, A., Pistolesi, M., Polacci Ripepe, M., Rossi, M., Scheu, E., Sulpizio, B., Tripoli, R., Valade, B., Valentine, S., Vidal, G., Wallentstein, C., N, 2016. MeMoVolc report on classification and dynamics of volcanic explosive eruptions. Bull. Volcanol. 78, 84. https://doi.org/10.1007/s00445-016-1071-y.

Bottari, A., Lo Giudice, E., Patané, G., Romano, R., Sturiale, C., 1975. L'eruzione etnea del Gennaio-Marzo 1974. Riv. Miner. Siciliana 154 (156), 175–199.

Branca, S., Del Carlo, P., 2004. Eruptions of Mt Etna during the past 3,200 years: a revised compilation integrating the historical and stratigraphic records. In: Bonaccorso, A., Calvari, S., Coltelli, M., Del Negro, C., Falsaperla, S. (Eds.), Mt. Etna: Volcano Laboratory. American Geophysical Union, Washington, DC, 143, pp. 1–27. https://doi.org/10.1029/143GM02.

Branca, S., Del Carlo, P., 2005. Types of eruptions of Etna volcano AD 1670–2003: implications for short-term eruptive behaviour. Bull. Volcanol. 67, 732–742. https://doi.org/10.1007/s00445-005-0412-z.

Branca, S., Coltelli, M., Groppelli, G., Lentini, F., 2011a. Geological map of Etna volcano, 1:50,000 scale. Ital. J. Geosci. 130 (3), 265–291. https://doi.org/10.3301/IJG.2011.15.

Branca, S., Coltelli, M., Groppelli, G., 2011b. Geological evolution of a complex basaltic stratovolcano: Mount Etna, Italye. Ital. J. Geosci. 130 (3), 306–317. https://doi.org/10.3301/IJG.2011.13.

Bursik, M., 2001. Effect of wind on the rise height of volcanic plumes. Geophys. Res. Lett. 28, 3621–3624. https://doi.org/10.1029/2001GL013393.

Burton, M.R., Neri, M., Andronico, D., Branca, S., Caltabiano, T., Calvari, S., Corsaro, R. A., Del Carlo, P., Lanzafame, G., Lodato, L., Miraglia, L., Salerno, G., Spampinato, L., 2005. Etna 2004-2005: an archetype for geodynamically-controlled effusive eruptions. Geophys. Res. Lett. 32, L09303 https://doi.org/10.1029/2005GL022527.

Calvari, S., Coltelli, M., Pompilio, M., Scribano, V., 1989. Attività dei Crateri Sommitali dell'Etna nel periodo 1987–1989 e petrochimica dei prodotti emessi. Boll. GNV 2, 697–714.

Calvari, S., Coltelli, M., Pompilio, M., Scribano, V., 1991. The eruptive activity between October 1989 and December 1990. Acta Vulcanol. 1, 257–260.

Calvari, S., Coltelli, M., Neri, M., Pompilio, M., Scribano, V., 1994. The 1991–1993 Etna eruption: chronology and lava flow-field evolution. Acta Vulcanol. 4, 1–14.

Calvari, S., Cannavò, F., Bonaccorso, A., Spampinato, L., Pellegrino, A.G., 2018. Paroxysmal explosions, lava fountains and ash plumes at Etna Volcano: eruptive processes and hazard implications. Front. Earth Sci. 6, 107. https://doi.org/10.3389/feart.2018.00107.

Cannata, A., Catania, A., Alparone, S., Gresta, S., 2008. Volcanic tremor at Mt. Etna: Inferences on magma dynamics during effusive and explosive activity. J. Volcanol. Geotherm. Res. 178, 19–31. https://doi.org/10.1016/j.jvolgeores.2007.11.027.

Cannavo, F., Sciotto, M., Cannata, A., Di Grazia, G., 2019. An integrated geophysical approach to track magma intrusion: the 2018 Christmas Eve eruption at Mount Etna. Geophys. Res. Lett. 46, 8009–8017. https://doi.org/10.1029/2019GL083120.

Cappello, A., Ganci, G., Bilotta, G., Herault, A., Zago, V., Del Negro, C., 2019a. Satellite-driven modeling approach for monitoring lava flow hazards during the 2017 Etna eruption. Ann. Geophys. 62 (2), VO227. https://doi.org/10.4401/ag-7792.

Cappello, A., Ganci, G., Bilotta, G., Corradino, C., Herault, A., Del Negro, C., 2019b. Changing eruptive styles at the South-East Crater of Mount Etna: Implications for assessing lava flow hazards. Front. Earth Sci. 2019, 7. https://doi.org/10.3389/feart.2019.00213.

Carveni, P., Romano, R., Caltabiano, T., Grasso, M.F., Gresta, S., 1994. The exceptional explosive activity of 5 January 1990 at the SE-Crater of Mt. Etna volcano (Sicily). Ital. J. Geosci. 113, 613–631.

CNR-IIV, 1989a. Rapporto sull'attività dell'Etna. Consiglio Nazionale delle Ricerche, Istituto Internazionale di Vulcanologia. Second quarter, 2/89.

CNR-IIV, 1989b. Rapporto sull'attività dell'Etna. Consiglio Nazionale delle Ricerche, Istituto Internazionale di Vulcanologia. Third quarter, 3/89.

CNR-IIV, 1989c. Rapporto sull'attività dell'Etna. Consiglio Nazionale delle Ricerche, Istituto Internazionale di Vulcanologia. Fourth quarter, 4/89.

CNR-IIV, 1989d. Rapporto Attività Etna. Consiglio Nazionale delle Ricerche, Istituto Internazionale di Vulcanologia (1989, Sett. Ott.).

CNR-IIV, 1995. The Current State of Mt. Etna Volcano. Consiglio Nazionale delle Ricerche, Istituto Internazionale di Vulcanologia. Fourth quarter, 4/95.

CNR-IIV, 1996a. The Current State of Mt. Etna Volcano. Consiglio Nazionale delle Ricerche, Istituto Internazionale di Vulcanologia. First quarter, 1/96.

CNR-IIV, 1996b. The Current State of Mt. Etna Volcano. Consiglio Nazionale delle Ricerche, Istituto Internazionale di Vulcanologia. Second quarter, 2/96.

CNR-IIV, 1998a. The Current State of Mt. Etna Volcano. Consiglio Nazionale delle Ricerche, Istituto Internazionale di Vulcanologia. First quarter, 1/98.

CNR-IIV, 1998b. The Current State of Mt. Etna Volcano. Consiglio Nazionale delle Ricerche, Istituto Internazionale di Vulcanologia. Third quarter, 3/98.

CNR-IIV, 1998c. The Current State of Mt. Etna Volcano. Consiglio Nazionale delle Ricerche, Istituto Internazionale di Vulcanologia. Fourth quarter, 4/98.

CNR-IIV, 1999. The Current State of Mt. Etna Volcaeno. Consiglio Nazionale delle Ricerche, Istituto Internazionale di Vulcanologia. First quarter, 1/99.

Coltelli, M., Del Carlo, P., Vezzoli, L., 1998. Discovery of a Plinian basaltic eruption of Roman age at Mt. Etna. Geology 26, 1095–1098. https://doi.org/10.1130/0091-7613(1998)026<1095:DOAPBE>2.3.CO;2.

Coltelli, M., Del Carlo, P., Vezzoli, L., 2000. Stratigraphic constraints for explosive activity in the last 100 ka at Etna volcano, Italy. Int. J. Earth Sci. 89, 665–677. https://doi.org/10.1007/s005310000117.

Coltelli, M., Proietti, C., Branca, S., Marsella, M., Andronico, D., Lodato, L., 2007. Analysis of the 2001 lava flow eruption of Mt. Etna from three-dimensional mapping. J. Geophys. Res. Earth Surf. 112 (F02029), 1–18. https://doi.org/10.1029/2006JF000598.

Corradini, S., Guerrieri, L., Lombardo, V., Merucci, L., Musacchio, M., Prestifilippo, M., Scollo, S., Silvestri, M., Spata, G., Stelitano, D., 2018. Proximal monitoring of the 2011–2015 Etna lava fountains using MSG-SEVIRI data. Geosciences 8, 140. https://doi.org/10.3390/geosciences8040140.

Corsaro, R.A., Andronico, D., Behncke, B., Branca, S., De Beni, E., Caltabiano, T., Ciancitto, F., Cristaldi, A., La Spina, A., Lodato, L., Giammanco, S., Miraglia, L., Neri, M., Salerno, G., Scollo, S., Spada, G., 2017. Monitoring the December 2015 summit eruptions of Mt. Etna (Italy): implications on eruptive dynamics. J. Volcanol. Geotherm. Res. 341, 53–69. https://doi.org/10.1016/j.jvolgeores.2017.04.018.

D'Agostino, M., Di Grazia, G., Ferrari, F., Langer, H., Messina, A., Reitano, D., Spampinato, S., 2013. Volcano monitoring and early warning on Mt Etna, sicily based on volcanic Tremor - methods and technical aspects. In: Zobin, V. (Ed.), Complex Monitoring of Volcanic Activity: Methods and Results. Nova Science Publishers, New York, USA. ISBN: 978-1-62417-985-3.

De Beni, E., Behncke, B., Branca, S., Nicolosi, I., Carluccio, R., Caracciolo D'Ajello, F., Chiappini, M., 2015. The continuing story of Etna's New Southeast Crater (2012–2014): evolution and volume calculations based on field surveys and aerophotogrammetry. J. Volcanol. Geotherm. Res. 303, 175–186. https://doi.org/10.1016/j.jvolgeores.2015.07.021.

De Beni, E., Cantarero, M., Neri, M., Messina, A., 2020. Lava flows of Mt Etna, Italy: the 2019 eruption within the context of the last two decades (1999–2019). J. Maps. https://doi.org/10.1080/17445647.2020.1854131.

DeRoin, N., McNutt, S.R., Thompson, G., 2015. Duration-amplitude relationships of volcanic tremor and earthquake swarms preceding and during the 2009 eruption of Redoubt volcano, Alaska. J. Volcanol. Geotherm. Res. 292, 56–69. https://doi.org/10.1016/j.jvolgeores.2015.01.003.

Di Grazia, G., Cannata, A., Montalto, P., Patanè, D., Privitera, E., Zuccarello, L., Boschi, E., 2009. A multiparameter approach to volcano monitoring based on 4D analyses of seismo-volcanic and acoustic signals: the 2008 Mt. Etna eruption. Geophys. Res. Lett. 36, L18307 https://doi.org/10.1029/2009GL039567.

Dinardo, G., Fabbiano, L., Vacca, G., 2013. Fluid flow rate estimation using acceleration sensors. In: 2013 Seventh International Conference on Sensing Technology (ICST), pp. 221–225. https://doi.org/10.1109/ICSensT.2013.6727646.

Donnadieu, F., Freville, P., Hervier, C., Coltelli, M., Scollo, S., Prestifilippo, M., Valade, S., Rivet, S., Cacault, P., 2016. Near-source Doppler radar monitoring of tephra plumes at Etna. J. Volcanol. Geotherm. Res. 312, 26–39. https://doi.org/10.1016/j.jvolgeores.2016.01.009.

Dubosclard, G., Cordesses, R., Allard, P., Hervier, C., Coltelli, M., Kornprobst, J., 1999. First testing of a volcano Doppler radar (Voldorad) at Mt. Etna. Geophys. Res. Lett. 26, 3389–3392. https://doi.org/10.1029/1999GL008371.

Eaton, J.P., Richter, D.H., Krivoy, H.L., 1987. Cycling of magma between the summit reservoir and Kilauea Iki lava lake during the 1959 eruption of Kilauea volcano. In: Decker, R.W., Wright, T.L., Stauffer, P.H. (Eds.), Volcanism in Hawaii. Geol. Surv. Prof. Pap, U.S.A., pp. 1307–1335

Edwards, M.J., Pioli, L., Andronico, D., Scollo, S., Ferrari, F., Cristaldi, A., 2018. Shallow factors controlling the explosivity of basaltic magmas: the 17–25 May 2016 eruption of Etna Volcano (Italy). J. Volcanol. Geotherm. Res. 357, 425–436. https://doi.org/10.1016/j.jvolgeores.2018.05.015.

Fee, D., Haney, M.M., Matoza, R.S., Van Eaton, A.R., Cervelli, P., Schneider, D.J., Iezzi, A.M., 2017. Volcanic tremor and plume height hysteresis from Pavlof Volcano, Alaska. Science 355 (6320), 45–48. https://doi.org/10.1126/science.aah6108.

Ferrucci, F., Rasà, R., Gaudiosi, G., Azzaro, R., Inposa, S., 1993a. Mt. Etna: a model for the 1989 eruption. J. Volcanol. Geotherm. Res. 56, 35–36.

Folch, A., Costa, A., Macedonio, G., 2016. FPLUME-1.0: An integral volcanic plume model accounting for ash aggregation. Geosci. Model Dev. 9, 431–450. https://doi.org/10.5194/gmd-9-431-2016.

Fornaciai, A., Andronico, D., Favalli, M., Spampinato, L., Branca, S., Lodato, L., Bonforte, A., Nannipieri, L. The 2004-05 Mt. Etna compound lava flow field: a retrospective analysis by combining remote and field methods. In print, Journal of Geophysical Research - Solid Earth, 126, e2020JB020499. doi:10.1029/2020JB020499.

Gestrich, J.E., Fee, D., Tsai, V.C., Haney, M.M., Van Eaton, A.R., 2020. A physical model for volcanic eruption tremor. J. Geophys. Res. Solid Earth 125. https://doi.org/10.1029/2019JB018980 e2019JB018980.

Giammanco, S., Sims, K.W.W., Neri, M., 2007. Measurements of ^{220}Rn and ^{222}Rn and CO_2 emissions in soil and fumarole gases on Mt. Etna volcano (Italy): implications for gas transport and shallow ground fracture. Geochem. Geophys. Geosyst. 8, Q10001. https://doi.org/10.1029/2007GC001644.

Global Volcanism Program, 1986. Report on Etna (Italy). In: McClelland, L. (Ed.), Scientific Event Alert Network Bulletin, 11. Smithsonian Institution, p. 9. https://doi.org/10.5479/si.GVP.SEAN198609-211060.

Global Volcanism Program, 1999. Report on Etna (Italy). In: Wunderman, R. (Ed.), Bulletin of the Global Volcanism Network, 24. Smithsonian Institution, p. 9. https://doi.org/10.5479/si.GVP.BGVN199909-211060.

Global Volcanism Program, 2013. In: Venzke, E. (Ed.), Volcanoes of the World, v. 4.8.8 (17 Apr 2020). Smithsonian Institution. https://doi.org/10.5479/si.GVP.VOTW4-2013. Downloaded 12 May 2020.

Gresta, S., Lombardo, G., Cristofolini, R., 1996. Characteristics of volcanic tremor accompanying the September 24th, 1986 explosive eruption of Mt. Etna (Italy). Ann. Geophys. 39 (2), 411–420. https://doi.org/10.4401/ag-3976.

Guest, J.E., 1982. Styles of eruption and flow morphology on Mt. Etna. Mem. Soc. Geol. It. 23, 49–73.

Guidoboni, E., Ciuccarelli, C., Mariotti, D., Comastri, A., Bianchi, M.G., 2014. L'Etna nella Storia. Catalogo delle eruzioni dall'antichità alla fine del XVII secolo. Bononia University Press.

Gutenberg, B., Richter, C.F., 1954. Magnitude and energy of earthquakes. Ann. Geofis. 9, 1–15. https://doi.org/10.4401/ag-5590.

Harris, A.J.L., Neri, M., 2002. Volumetric observations during paroxysmal eruptions at Mount Etna: pressurized drainage of a shallow chamber or pulsed supply? J. Volcanol. Geotherm. Res. 116, 79–95. https://doi.org/10.1016/S0377-0273(02)00212-3.

Harris, A., Steffke, A., Calvari, S., Spampinato, L., 2011. Thirty years of satellite-derived lava discharge rates at Etna: Implications for steady volumetric output. J. Geophys. Res. 116, B08204 https://doi.org/10.1029/2011JB008237.

Houghton, B.F., Taddeucci, J., Andronico, D., Gonnerman, H.M., Pistolesi, M., Patrick, M.R., Orr, T.R., Swanson, D.A., Edmonds, M., Gaudin, D., Carey, R.J., Scarlato, P., 2016. Stronger or longer: Discriminating between Hawaiian and Strombolian eruption styles. Geology 44 (2), 163–166. https://doi.org/10.1130/G37423.1.

Horwell, C.J., Sargent, P., Andronico, D., Lo Castro, M.D., Tomatis, M., Hillman, S.E., Michnowicz, S.A.K., Fubini, B., 2017. The iron-catalysed surface reactivity and health-pertinent physical characteristics of explosive volcanic ash from Mt. Etna, Italy. J. Appl. Volcanol. 6, 12. https://doi.org/10.1186/s13617-017-0063-8.

Ichihara, M., 2016. Seismic and infrasonic eruption tremors and their relation to magma discharge rate: a case study for sub-Plinian events in the 2011 eruption of Shinmoedake, Japan. J. Geophys. Res. Solid Earth 121, 7101–7118. https://doi.org/10.1002/2016JB013246.

INGV-OE, 2019a. Bollettino settimanale sul monitoraggio vulcanico, geochimico e sismico del vulcano Etna. 27/05/2019–02/06/2019. Rep. N° 23/2019. Available at: http://www.ct.ingv.it/en/rapporti/multidisciplinari.html?view=docman.

INGV-OE, 2019b. Bollettino settimanale sul monitoraggio vulcanico, geochimico e sismico del vulcano Etna. 03/06/2019–09/06/2019. Rep. N° 24/2019. Available at: http://www.ct.ingv.it/en/rapporti/multidisciplinari.html?view=docman.

INGV-OE, 2019c. Bollettino settimanale sul monitoraggio vulcanico, geochimico e sismico del vulcano Etna. 15/07/2019–21/07/2019. Rep. N° 30/2019. Available at: http://www.ct.ingv.it/en/rapporti/multidisciplinari.html?view=docman.

INGV-OE, 2020a. Bollettino settimanale sul monitoraggio vulcanico, geochimico e sismico del vulcano Etna. 23/11/2020–29/11/2020. Rep. N° 49/2020. Available at: https://www.ct.ingv.it/index.php/monitoraggio-e-sorveglianza/prodotti-del-monitoraggio/bollettini-settimanali-multidisciplinari/404-bollettino-settimanale-sul-monitoraggio-vulcanico-geochimico-e-sismico-del-vulcano-Stromboli20201229/file.

INGV-OE, 2020b. Bollettino settimanale sul monitoraggio vulcanico, geochimico e sismico del vulcano Etna. 18/05/2020–24/05/2020. Rep. N° 22/2020. Available at. https://www.ct.ingv.it/index.php/monitoraggio-e-sorveglianza/prodotti-del-monitoraggio/bollettini-settimanali-multidisciplinari/337-bollettino-settimanale-sul-monitoraggio-vulcanico-geochimico-e-sismico-del-vulcano-etna20200526/file.

Jaupart, C., Vergniolle, S., 1988. Laboratory models of Hawaiian and Strombolian eruptions. Nature 331, 58–60.

Jaupart, C., Vergniolle, S., 1989. The generation and collapse of foam layer at the roof of a basaltic magma chamber. J. Fluid Mech. 203, 347–380.

Konstantinou, K.I., Astrid Ardiani, M., Sudiby, M.R.P., 2019. Scaling behaviour and source mechanism of tremor recorded at Erebus volcano, Ross island, Antarctica. Phys. Earth Planet. Inter. 290, 99–106. https://doi.org/10.1016/j.pepi.2019.03.010.

La Spina, A.L., Burton, M.R., Allard, P., Alparone, S., Muré, F., 2015. Open-path FTIR spectroscopy of magma degassing processes during eight lava fountains on Mount Etna. Earth Planet. Sci. Lett. 413, 123–134. https://doi.org/10.1016/j.epsl.2014.12.038.

Laiolo, M., Ripepe, M., Cigolini, C., Coppola, D., Della, S.M., Genco, R., Innocenti, L., Lacanna, G., Marchetti, E., Massimetti, F., Silengo, M.C., 2019. Space- and ground-based geophysical data tracking of magma migration in shallow feeding system of Mount Etna volcano. Remote Sens. 11, 1182. Special Issue "Remote Sensing of Volcanic Processes and Risk". https://doi.org/10.3390/rs11101182.

Mazzarini, F., Armienti, P., 2001. Flank cones at Mount Etna volcano: do they have a power-law distribution? Bull. Volcanol. 62, 420–430. https://doi.org/10.1007/s004450000109.

McNutt, S.R., 1994. Volcanic tremor amplitude correlated with volcano explosivity and its potential use in determining ash hazards to aviation. U.S. Geol. Survey Bull. 2047, 377–385.

McNutt, S.R., 2005. Volcanic seismology. Annu. Rev. Earth Planet. Sci. 32, 461–491. https://doi.org/10.1146/annurev.earth.33.092203.122459.

McNutt, S.R., Nishimura, T., 2008. Volcanic tremor during eruptions: temporal characteristics, scaling and constraints on conduit size and processes. J. Volcanol. Geotherm. Res. 178, 10–18. https://doi.org/10.1016/j.jvolgeores.2008.03.010.

Métrich, N., Allard, P., Spilliaert, N., Andronico, D., Burton, M., 2004. 2001 flank eruption of the alkali- and volatile-rich primitive basalt responsible for Mount Etna's evolution in the last three decades. Earth Planet. Sci. Lett. 228, 1–17. https://doi.org/10.1016/j.epsl.2004.09.036.

Neri, M., Maio, M.D., Crepaldi, S., Suozzi, E., Lavy, M., Marchionatti, F., Calvari, S., Buongiorno, M.F., 2017. Topographic maps of Mount Etna's summit craters, updated to December 2015. J. Maps 13 (2), 674–683. https://doi.org/10.1080/17445647.2017.1352041.

Osman, S., Rossi, E., Bonadonna, C., Frischknecht, C., Andronico, D., Cioni, R., Scollo, S., 2019. Exposure-based risk assessment and emergency management associated with the fallout of large clasts at Mount Etna. Nat. Hazards Earth Syst. Sci. 19, 589–610. https://doi.org/10.5194/nhess-19-589-2019.

Parfitt, E.A., 2004. A discussion of the mechanisms of explosive basaltic eruptions. J. Volcanol. Geotherm. Res. 134 (1–2), 77–107.

Parfitt, E.A., Wilson, L., 1995. Explosive volcanic eruptions: IX. The transition between Hawaiian-style lava fountaining and Strombolian explosive activity. Geophys. J. Int. 121, 226–232.

Patanè, D., Di Grazia, G., Cannata, A., Montalto, P., Boschi, E., 2008. Shallow magma pathway geometry at Mt. Etna volcano. Geochem. Geophys. Geosyst. 9, Q12021 https://doi.org/10.1029/2008GC002131.

Patanè, D., Aiuppa, A., Aloisi, M., Behncke, B., Cannata, A., Coltelli, M., Di Grazia, G., Gambino, S., Gurrieri, S., Mattia, M., Salerno, G., 2013. Insights into magma and fluid transfer at Mount Etna by a multiparametric approach: a model of the events leading to the 2011 eruptive cycle. J. Geophys. Res. 118, 7. https://doi.org/10.1002/jgrb.50248.

Polacci, M., Burton, M.R., La Spina, A., Murè, F., Favretto, S., Zanini, F., 2009. The role of syn-eruptive vesiculation on explosive basaltic activity at Mt. Etna, Italy. J. Volcanol. Geotherm. Res. 179, 265–269. https://doi.org/10.1016/j.jvolgeores.2008.11.026.

Poret, M., Corradini, S., Merucci, L., Costa, A., Andronico, D., Montopoli, M., Vulpiani, G., Freret-Lorgeril, V., 2018a. Reconstructing volcanic plume evolution integrating satellite and ground-based data: application to the 23 November 2013 Etna eruption. Atmos. Chem. Phys. 18, 4695–4714. https://doi.org/10.5194/acp-18-4695-2018.

Poret, M., Costa, A., Andronico, D., Scollo, S., Gouhier, M., Cristaldi, A., 2018b. Modeling eruption source parameters by integrating field, ground-based, and satellite-based measurements: The case of the 23 February 2013 Etna paroxysm. J. Geophys. Res. Solid Earth 123. https://doi.org/10.1029/2017JB015163.

Privitera, E., Sgroi, T., Gresta, S., 2003. Statistical analysis of intermittent volcanic tremor associated with the September 1989 summit explosive eruptions at Mount Etna, Sicily. J. Volcanol. Geotherm. Res. 120 (3–4), 235–247. https://doi.org/10.1016/S0377-0273(02)00400-6.

Rittmann, A., 1973. Structure and evolution of Mount Etna. Philos. Trans. R. Soc. Lond. 274, 5–16.

Romano, R., 1989. Annual report of the world volcanic eruptions in 1986. Bull. Volc. Erupt. 26, 3–5.

Salerno, G.G., Burton, M., Di Grazia, G., Caltabiano, T., Oppenheimer, C., 2018. Coupling between magmatic degassing and volcanic tremor in basaltic volcanism. Front. Earth Sci. 6, 157. https://doi.org/10.3389/feart.2018.00157.

Sandanbata, O., Obara, K., Maeda, T., Takagi, R., Satake, K., 2015. Sudden changes in the amplitude-frequency distribution of long-period tremors at Aso volcano, southwest Japan. Geophys. Res. Lett. 42, 10256–10262. https://doi.org/10.1002/2015GL066443.

Sciotto, M., Cannata, A., Prestifilippo, M., Scollo, S., Fee, D., Privitera, E., 2019. Unravelling the links between seismo-acoustic signals and eruptive parameters: Etna lava fountain case study. Sci. Rep. 9, 16417. https://doi.org/10.1038/s41598-019-52576-w.

Scollo, S., Del Carlo, P., Coltelli, M., 2007. Tephra fallout of 2001 Etna flank eruption: analysis of the deposit and plume dispersion. J. Volcanol. Geotherm. Res. 160, 147–164. https://doi.org/10.1016/j.jvolgeores.2006.09.007.

Scollo, S., Prestifilippo, M., Pecora, E., Corradini, S., Merucci, L., Spata, G., Coltelli, M., 2014. Eruption column height estimation of the 2011–2013 Etna lava fountains. Ann. Geophys. 57 (2) https://doi.org/10.4401/ag-6396.

Spampinato, L., Sciotto, M., Cannata, A., Cannavò, F., La Spina, A., Palano, M., Salerno, G.G., Privitera, E., Caltabiano, T., 2015. Multiparametric study of the February–April 2013 paroxysmal phase of Mt. Etna New South-East crater. Geochem. Geophys. Geosyst. 15 (6) https://doi.org/10.1002/2015GC005795.

Sparks, R.S.J., Bursik, M.I., Carey, S.N., Gilbert, J.S., Glaze, L.S., Sigurdsson, H., Woods, A.W., 1997. Volcanic Plumes. John Wiley & Sons, Chichester, p. 574.

Spina, L., Taddeucci, J., Cannata, A., Sciotto, M., Del Bello, E., Scarlato, P., Kueppers, U., Andronico, D., Privitera, E., Ricci, T., Pena-Fernandez, J., Sesterhenn, J., Dingwell, D.B., 2017. Time-series analysis of fissure-fed multi-vent activity: a snapshot from the July 2014 eruption of Etna volcano (Italy). Bull. Volcanol. 79, 51. https://doi.org/10.1007/s00445-017-1132-x.

Spina, L., Cannata, A., Morgavi, D., Perugini, D., 2019. Degassing behaviour at basaltic volcanoes: new insights from experimental investigations of different conduit geometry and magma viscosity. Earth Sci. Rev. 192, 317–336. https://doi.org/10.1016/j.earscirev.2019.03.010.

Taddeucci, J., Pompilio, M., Scarlato, P., 2002. Monitoring the explosive activity of the July–August 2001 eruption of Mt. Etna (Italy) by ash characterization. Geophys. Res. Lett. 29, 1029–1032. https://doi.org/10.1029/2001GL014372.

Trnkoczy, A., 2012. Understanding and parameter setting of STA/LTA trigger algorithm. In: Bormann, P. (Ed.), IASPEI New Manual of Seismological Observatory Practice 2 (NMSOP-2). IASPEI, Potsdam, pp. 1–20. https://doi.org/10.2312/GFZ. NMSOP-2_IS_8.1.

Vergniolle, S., Jaupart, C., 1990. Dynamics of degassing at Kilauea volcano, Hawaii. J. Geophys. Res. 95, 2793–2809.Vergniolle, S., 1996. Bubble size distribution in magma chambers and dynamics of basaltic eruptions. Earth Planet. Sci. Lett. 140, 269–279.

Viccaro, M., Garozzo, I., Cannata, A., Di Grazia, G., Gresta, S., 2014. Gas burst vs. gas-rich magma recharge: a multidisciplinary study to reveal factors controlling duration of the recent paroxysmal eruptions at Mt. Etna. J. Volcanol. Geotherm. Res. 278–279, 1–13. https://doi.org/10.1016/j.jvolgeores.2014.04.001.

VONA, 2021a. Volcano Observatory Notice for Aviation (VONA). Issued on 2021-02-16 17:05:25. Available at: https://www.ct.ingv.it/Dati/informative/vona/VONA_ETNA_202102161705Z_2021001106C02.pdf.

VONA, 2021b. Volcano Observatory Notice for Aviation (VONA). Issued on 2021-02-19 09:47:17. Available at: https://www.ct.ingv.it/Dati/informative/vona/VONA_ETNA_202102190947Z_2021001706C04.pdf.

VONA, 2021c. Volcano Observatory Notice for Aviation (VONA). Issued on 2021-02-28 08:35:34. Available at: https://www.ct.ingv.it/Dati/informative/vona/VONA_Etna_202102280835Z_2021002706C06.pdf.

VONA, 2021d. Volcano Observatory Notice for Aviation (VONA). Issued on 2021-03-02 13:17:03. Available at: https://www.ct.ingv.it/Dati/informative/vona/VONA_Etna_202103021317Z_2021003106C07.pdf.

VONA, 2021e. Volcano Observatory Notice for Aviation (VONA). Issued on 2021-03-04 08:17:04. Available at: https://www.ct.ingv.it/Dati/informative/vona/VONA_Etna_202103040817Z_2021003606C09.pdf.

VONA, 2021f. Volcano Observatory Notice for Aviation (VONA). Issued on 2021-03-07 06:30:06. Available at: https://www.ct.ingv.it/Dati/informative/vona/VONA_Etna_202103120749Z_2021004606E51.pdf.

VONA, 2021h. Volcano Observatory Notice for Aviation (VONA). Issued on 2021-03-12 08:44:05. Available at: https://www.ct.ingv.it/Dati/informative/vona/VONA_Etna_202103120844Z_2021004706C10.pdf.

VONA, 2021i. Volcano Observatory Notice For Aviation (VONA). Issued on 2021-03-24 03:45:17. Available at: https://www.ct.ingv.it/Dati/informative/vona/VONA_Etna_202103240345Z_2021006106C14.pdf.

VONA, 2021j. Volcano Observatory Notice for Aviation (VONA). Issued on 2021-04-01 07:47:35. Available at: https://www.ct.ingv.it/Dati/informative/vona/VONA_Etna_202104010747Z_2021006706C17.pdf.

VONA, 2021g. Volcano Observatory Notice for Aviation (VONA). Issued on 2021-03-10 00:56:40. Available at: https://www.ct.ingv.it/Dati/informative/vona/VONA_Etna_202103100056Z_2021004306E49.pdf.

Vulpiani, G., Ripepe, M., Valade, S., 2016. Mass discharge rate retrieval combining weather radar and thermal camera observations. J. Geophys. Res. Solid Earth 121, 5679–5695. https://doi.org/10.1002/2016jb013191.

Wilson, L., Sparks, R.S.J., Walker, G.P.L., 1980. Explosive volcanic eruptions — IV. The control of magma properties and conduit geometry on eruption column behaviour. Geophys. J. R. Astron. Soc. 63, 117–148. https://doi.org/10.1111/j.1365-246X.1980.tb02613.x.

Yukutake, Y., Honda, R., Harada, M., Doke, R., Saito, T., Ueno, T., Sakai, S., Morita, Y., 2017. Analyzing the continuous volcanic tremors detected during the 2015 phreatic eruption of the Hakone volcano. Earth Planets Space 69, 164. https://doi.org/10.1186/s40623-017-0751-y.